

# Phase gate of one qubit simultaneously controlling $n$ qubits in a cavity or coupled to a resonator

Chui-Ping Yang,<sup>1,2</sup> Yu-xi Liu,<sup>3,4,1</sup> and Franco Nori<sup>1,2</sup>

<sup>1</sup>*Advanced Science Institute, The Institute of Physical and Chemical Research (RIKEN), Wako-Shi, Saitama 351-0198, Japan*

<sup>2</sup>*Physics Department, The University of Michigan, Ann Arbor, Michigan 48109-1040, USA*

<sup>3</sup>*Institute of Microelectronics, Tsinghua University, Beijing 100084, China*

<sup>4</sup>*Tsinghua National Laboratory for Information Science and Technology (TNList), Tsinghua University, Beijing 100084, China*

(Dated: October 12, 2019)

We propose how to realize a three-step controlled-phase gate of one qubit simultaneously controlling  $n$  qubits in a cavity or coupled to a resonator. The  $n$  two-qubit controlled-phase gates forming this "multi-qubit phase gate" can be performed simultaneously. The operation time of this gate is independent of the number  $n$  of qubits. This phase gate controlling at once  $n$  qubits is insensitive to the initial state of the cavity mode and can be used to produce an analogous CNOT gate, simultaneously acting on  $n$  qubits. We present two alternative approaches to implement this gate. One approach is based on tuning the qubit frequency while the other method tunes the resonator frequency. Using superconducting qubits coupled to a resonator as an example, we show how to implement the proposed gate. We also give a discussion on realizing the proposed gate with atoms and preparing multiple atoms in an entangled state (*with an arbitrary entanglement degree*), by using one cavity initially in an arbitrary state.

PACS numbers: 03.67.Lx, 42.50.Dv, 85.25.Cp

## I. INTRODUCTION

Quantum information processing has attracted considerable interest during the past decade. The building blocks of quantum computing are single-qubit and two-qubit logic gates. So far, a large number of theoretical proposals for realizing two-qubit gates in many physical systems have been proposed. Moreover, two-qubit controlled-not (CNOT) or controlled-phase (CP) gates have been experimentally demonstrated in, e.g., cavity QED [1,2], ion traps [3], NMR [4], quantum dots [5], and superconducting qubits [6,7].

Attention is now shifting to the physical realization of multi-qubit controlled gates (e.g., in Ref. [8]) instead of just two-qubit gates. It is known that multi-qubit controlled gates play a significant role in constructing network quantum computation circuits. When using the conventional gate-decomposition protocols to construct a multi-qubit controlled gate [9,10], the procedure usually becomes complicated (especially for large  $n$ ), as the number of single-qubit and two-qubit gates required for the gate implementation heavily depends on the number  $n$  of qubits. Therefore, building a multi-qubit controlled gate may become very difficult since each elementary gate requires turning on and off a given Hamiltonian for a certain period of time, and each additional basic gate adds experimental complications and the possibility of more errors.

Several methods for constructing phase gates with  $n$ -control qubits acting on one target qubit based on cavity QED or ion traps have been recently proposed [11-14]. These methods open a new way for realizing quantum controlled-phase gates with multiple control qubits. However, we note that these proposals [11-14] cannot be extended to perform a different type of significant multi-qubit controlled-phase gate, i.e., quantum controlled-phase gates with one qubit controlling  $n$  target qubits.

In this work, we propose a way for realizing a three-step controlled-phase gate of one qubit simultaneously controlling  $n$  qubits in a cavity or coupled to a resonator. To achieve this, we construct an effective Hamiltonian which contains interaction terms between the control qubit and each subordinate or target qubit. We will denote this  $n$ -target-qubit control-phase gate as a NTCP gate [Fig. 1(a)]. We present two alternative approaches to implement this NTCP gate. One approach is based on tuning the qubit frequency while the other method tunes the cavity (or resonator) frequency. We present these two alternative methods because some experimental implementations might find it easier to tune the qubit frequency, while others might prefer to tune the cavity frequency. For solid state qubits such as superconducting qubits and semiconductor quantum dots, the qubit transition frequency (or the qubit level spacings) can be readily adjusted by varying the external parameters [15-20]. And, the cavity mode frequency  $\omega_c$  can be changed in various experiments (e.g., [21-25]). In addition, for these two methods, we provide detailed guidelines on how to protect multi-level qubits from leaking out of the computational subspace. As discussed in the appendixes, the leakage out of the computational subspace can in principle be suppressed as long as the cavity mode and the pulses are largely detuned from the transition between the irrelevant energy levels.

As shown below, our proposal has the following advantages: (i) The  $n$  two-qubit CP gates involved in the NTCP

gate can be performed simultaneously; (ii) The operation time required for the gate implementation is independent of the number  $n$  of qubits; (iii) This proposal is insensitive to the initial state of the cavity mode, and thus no preparation for the initial state of the cavity mode is needed; (iv) The detunings ( $\delta$  and  $\delta'$ ) between the cavity mode and the qubits are not required to be larger than the qubit-cavity coupling constants ( $g$  and  $g'$ ); and (v) The proposal requires only three steps of operations.

Note that a CNOT gate of one qubit simultaneously controlling  $n$  qubits, shown in Fig. 1(b), can also be achieved using the present proposal. This is because the  $n$ -target-qubit CNOT gate is equivalent to a NTCP gate plus a single-qubit Hadamard gate acting on each target qubit before and after the NTCP gate [Fig. 1(b)].

To the best of our knowledge, our proposal is the first to demonstrate that a powerful phase gate, synchronously controlling  $n$  qubits, can be achieved in a cavity or resonator, which can be *initially in an arbitrary state*. This proposal is quite general and can be applied to physical systems such as trapped atoms, quantum dots, and superconducting qubits. We believe that this work is of general interest and significance because it provides a protocol for performing a controlled-phase (or controlled-not) gate with multiple target qubits, which is important in quantum information processing such as entanglement preparation [26], error correction [27], quantum algorithms (e.g., the Discrete Cosine Transform [28]), quantum cloning [29], and quantum information coding or spreading (see the discussion given in subsection VI. B).

This paper is organized as follows. In Sec. II, we introduce the  $n$ -target-qubit control phase gate studied in this work. In Sec. III, we discuss how to obtain the time-evolution operators for a qubit system interacting with a single cavity mode and driven by a classical pulse. In Sec. IV, using the time-evolution operators obtained, we present two alternative approaches for realizing the NTCP gate with qubits in a cavity or coupled to a resonator. In the appendixes, we provide detailed guidelines on how to protect multi-level qubits from leaking out of the computational subspace. In Sec. V, using superconducting qubits coupled to a resonator, we show how to apply our general proposal to implement the proposed NTCP gate, and then discuss its feasibility based on current experiments in superconducting quantum circuits. In Sec. VI, we discuss how to extend the present proposal to implement the NTCP gate with trapped atomic qubits, by the use of one cavity; and we further discuss how to prepare multiple atoms in an entangled state with an *arbitrary* entanglement degree, by using the present proposal. A concluding summary is provided in Sec. VII.

## II. ONE QUBIT SIMULTANEOUSLY CONTROLLING $N$ TARGET QUBITS

For two qubits, there are a total of four computational basis states, denoted by  $|00\rangle$ ,  $|01\rangle$ ,  $|10\rangle$ , and  $|11\rangle$ , respectively. A two-qubit CP gate is defined by

$$|00\rangle \rightarrow |00\rangle, |01\rangle \rightarrow |01\rangle, |10\rangle \rightarrow |10\rangle, |11\rangle \rightarrow -|11\rangle, \quad (1)$$

which implies that if and only if the control qubit (the first qubit) is in the state  $|1\rangle$ , a phase flip happens to the state  $|1\rangle$  of the target qubit (the second qubit), but nothing happens otherwise.

The NTCP gate considered here consists of  $n$  two-qubit CP gates [Fig. 1(a)]. Each two-qubit CP gate involved in this NTCP gate has a *shared* control qubit (labelled by 1) but a different target qubit (labelled by 2, 3, ..., or  $n+1$ ). According to the transformation (1) for a two-qubit CP gate, it can be seen that this NTCP gate with one control qubit (qubit 1) and  $n$  target qubits (qubits 2, 3, ...,  $n+1$ ) can be described by the following unitary operator

$$U_p = \prod_{j=2}^{n+1} (I_j - 2|1_1 1_j\rangle\langle 1_1 1_j|), \quad (2)$$

where the subscript 1 represents the control qubit 1, while  $j$  represents the target qubit  $j$ , and  $I_j$  is the identity operator for the qubit pair  $(1, j)$ , which is given by  $I_j = \sum_{rs} |r_1 s_j\rangle\langle r_1 s_j|$ , with  $rs = 00, 01, 10$ , or  $11$ . One can see that the operator (2) induces a phase flip (from the  $+$  sign to the  $-$  sign) to the logical state  $|1\rangle$  of each target qubit when the control qubit 1 is initially in the state  $|1\rangle$ , and nothing happens otherwise.

## III. MODEL AND UNITARY EVOLUTION

Consider  $(n+1)$  qubits interacting with the cavity mode and driven by a classical pulse. In the rotating-wave approximation, the Hamiltonian for the whole system is (assuming  $\hbar = 1$ )

$$H = H_0 + H_1 + H_2, \quad (3)$$

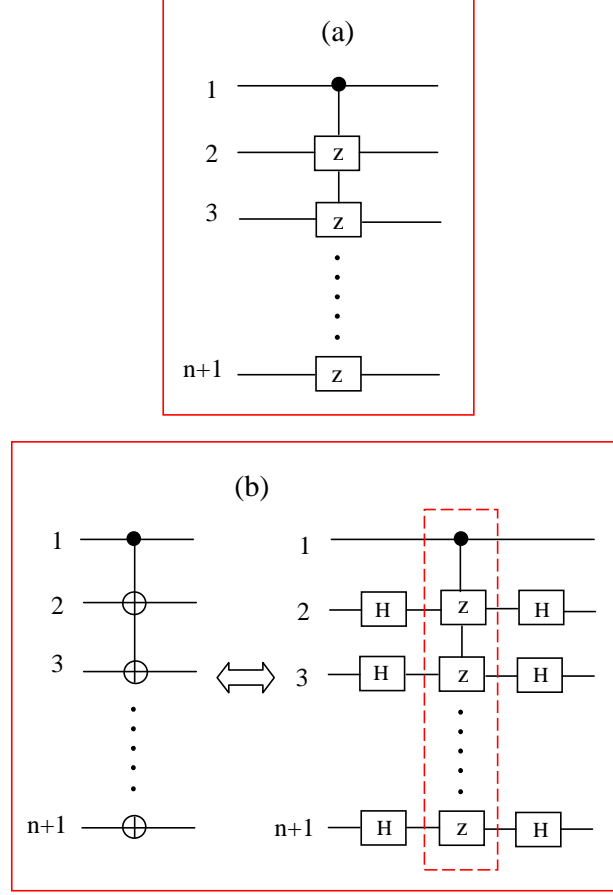


FIG. 1: (Color online) (a) Schematic circuit of a  $n$ -target-qubit control phase (NTCP) gate with qubit 1 simultaneously controlling  $n$  target qubits (2, 3, ...,  $n+1$ ). The NTCP gate is equivalent to  $n$  two-qubit control phase (CP) gates each having a shared control qubit (qubit 1) but a different target qubit (either qubit 2, 3, ..., or  $n+1$ ). Here,  $Z$  represents a controlled-phase flip on each target qubit. Namely, if the control qubit 1 is in the state  $|1\rangle$ , then the state  $|1\rangle$  at each  $Z$  is phase-flipped as  $|1\rangle \rightarrow -|1\rangle$ , while the state  $|0\rangle$  remains unchanged. (b) Relationship between a  $n$ -target-qubit controlled-NOT gate and a NTCP gate. The circuit on the left side of (b) is equivalent to the circuit on the right side of (b). For the circuit on the left side, the symbol  $\oplus$  represents a CNOT gate on each target qubit. If the control qubit 1 is in the state  $|1\rangle$ , then the state at  $\oplus$  is bit flipped as  $|1\rangle \rightarrow |0\rangle$  and  $|0\rangle \rightarrow |1\rangle$ . However, when the control qubit 1 is in the state  $|0\rangle$ , the state at  $\oplus$  remains unchanged. On the other hand, for the circuit on the right side, the part enclosed in the (red) dashed-line box represents a NTCP gate. The element containing  $H$  corresponds to a Hadamard transformation described by  $|0\rangle \rightarrow (1/\sqrt{2})(|0\rangle + |1\rangle)$ , and  $|1\rangle \rightarrow (1/\sqrt{2})(|0\rangle - |1\rangle)$ .

with

$$H_0 = -\frac{\omega_0}{2}S_z + \omega_c a^\dagger a, \quad (4)$$

$$H_1 = \frac{\Omega}{2} \left[ e^{i(\omega t + \varphi)} S_- + e^{-i(\omega t + \varphi)} S_+ \right], \quad (5)$$

$$H_2 = g(aS_+ + a^\dagger S_-). \quad (6)$$

Here,  $H_0$  is the free Hamiltonian of the qubits and the cavity mode,  $H_1$  is the interaction Hamiltonian between the qubits and the cavity mode, and  $H_2$  is the interaction Hamiltonian between the qubits and the classical pulse. In addition,  $\omega_0$  is the transition frequency between the two levels  $|0\rangle$  and  $|1\rangle$  of each qubit;  $a$  ( $a^\dagger$ ) is the photon annihilation (creation) operator of the cavity mode with frequency  $\omega_c$ ;  $g$  is the coupling constant between the cavity mode and each qubit;  $\Omega$ ,  $\omega$ , and  $\varphi$  are the Rabi frequency, the frequency, and the initial phase of the pulse, respectively;

and  $S_z$ ,  $S_-$ , and  $S_+$  are the collective operators for the  $(n+1)$  qubits, which are given by

$$S_z = \sum_{j=1}^{n+1} \sigma_{z,j}, \quad S_- = \sum_{j=1}^{n+1} \sigma_j^-, \quad S_+ = \sum_{j=1}^{n+1} \sigma_j^+ \quad (7)$$

where  $\sigma_{z,j} = |0\rangle_j \langle 0| - |1\rangle_j \langle 1|$ ,  $\sigma_j^- = |0\rangle_j \langle 1|$ , and  $\sigma_j^+ = |1\rangle_j \langle 0|$ , with  $|0\rangle_j$  and  $|1\rangle_j$  ( $j = 1, 2, \dots, n+1$ ) being the ground state and excited level of the  $j$ th qubit. The interaction Hamiltonians,  $H_1$  and  $H_2$ , in the interaction picture with respect to  $H_0$ , are given by (assuming  $\omega = \omega_0$ )

$$H_1 = \frac{\Omega}{2} (e^{i\varphi} S_- + e^{-i\varphi} S_+), \quad (8)$$

$$H_2 = g (e^{i\delta t} a S_+ + e^{-i\delta t} a^\dagger S_-), \quad (9)$$

where

$$\delta = \omega_0 - \omega_c \quad (10)$$

is the detuning between the  $|0\rangle \leftrightarrow |1\rangle$  transition frequency  $\omega_0$  of each qubit and the frequency  $\omega_c$  of the cavity mode.

We now consider two special cases:  $\varphi = \pi$  and negative detuning  $\delta < 0$ , as well as  $\varphi = 0$  and positive detuning  $\delta > 0$ . The detailed discussion of these two cases will be given in the following subsections III. A and III. B. The results from the unitary evolution, obtained for these two special cases, will be employed by the two alternative approaches (presented in next section) for the gate implementation.

#### A. Case for pulse phase $\varphi = \pi$ and detuning $\delta < 0$

In this subsection, we consider the negative detuning case  $\delta < 0$  [Fig. 2(a)]. When  $\varphi = \pi$ , the above Hamiltonian (8) reduces to

$$H_1 = -\frac{\Omega}{2} S_x, \quad (11)$$

where

$$S_x = S_- + S_+ = \sum_{j=1}^{n+1} \sigma_{x,j}, \quad (12)$$

with  $\sigma_{x,j} = \sigma_j^- + \sigma_j^+$ . Performing the unitary transformation  $|\psi(t)\rangle = e^{-iH_1 t} |\psi'(t)\rangle$ , we obtain

$$i \frac{d|\psi'(t)\rangle}{dt} = \overline{H}_2 |\psi'(t)\rangle, \quad (13)$$

with

$$\begin{aligned} \overline{H}_2 &= e^{iH_1 t} H_2 e^{-iH_1 t} \\ &= \frac{g}{2} \left\{ e^{i\delta t} a \left[ S_x + \frac{1}{2} (S_z - S_- + S_+) e^{-i\Omega t} - \frac{1}{2} (S_z + S_- - S_+) e^{i\Omega t} \right] \right\} + \text{H.c.}, \end{aligned} \quad (14)$$

Assuming that  $\Omega \gg |\delta|, g$ , we can neglect the fast-oscillating terms [30-32]. Then the Hamiltonian (14) reduces to [30-32]

$$\overline{H}_2 = \frac{g}{2} (e^{i\delta t} a + e^{-i\delta t} a^\dagger) S_x. \quad (15)$$

The evolution operator for the Hamiltonian (15) can be written in the form [14,30,33,34]

$$u(t) = e^{-iA(t)S_x^2} e^{-iB(t)S_x a} e^{-iB^*(t)S_x a^\dagger}, \quad (16)$$

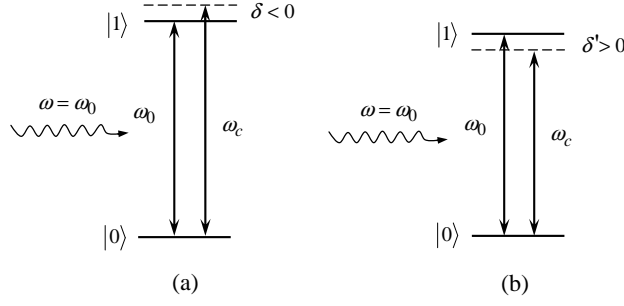


FIG. 2: Illustration of different detunings between the cavity mode frequency  $\omega_c$  and the qubit transition frequency  $\omega_0$ . Here,  $\omega_0$ ,  $\omega_c$ , and  $\omega$  are the qubit transition frequency, the cavity mode frequency, and the pulse frequency, respectively. In (a), the detuning  $\delta = \omega_0 - \omega_c < 0$ . In (b), the detuning  $\delta' = \omega_0 - \omega_c > 0$ . To implement a NTCP gate, we propose two alternative approaches (see section IV), each one with three steps. The first step for either method requires a negative detuning ( $\delta < 0$ ), as shown in (a). For either method, the second step requires a positive detuning ( $\delta' > 0$ ), as shown in (b).

where

$$\begin{aligned}
 B(t) &= \frac{g}{2} \int_0^t e^{i\delta t'} dt' = \frac{g}{2i\delta} (e^{i\delta t} - 1), \\
 A(t) &= i \int_0^t B(t') \frac{dB^*(t')}{dt'} dt' \\
 &= \frac{g^2}{4\delta} \left[ t + \frac{1}{i\delta} (e^{-i\delta t} - 1) \right].
 \end{aligned} \tag{17}$$

When the evolution time  $t$  satisfies  $t = \tau = 2\pi/|\delta|$ , we have  $B(\tau) = 0$  and  $A(\tau) = g^2\tau/(4\delta)$ . Then we obtain

$$u(\tau) = \exp(i\lambda\tau S_x^2), \tag{18}$$

where  $\lambda = -g^2/(4\delta) > 0$ . The evolution operator of the system (in the interaction picture with respect to  $H_0$ ) is thus given by

$$U(\tau) = e^{-iH_1\tau} u(\tau) = e^{i\Omega\tau S_x/2} e^{i\lambda\tau S_x^2}. \tag{19}$$

In section IV, we propose two alternative approaches for the NTCP gate implementation, each one involving three steps. The evolution operator (19) will be needed for the first step for either one of the two alternative approaches.

### B. Case for pulse phase $\varphi = 0$ and detuning $\delta > 0$

In the following, we consider the positive detuning case  $\delta > 0$ . The detuning  $\delta$  can be adjusted from  $\delta < 0$  to  $\delta > 0$  by changing *either* the qubit transition frequency  $\omega_0$  *or* the cavity mode frequency  $\omega_c$ , *or* both. In general, the qubit-cavity coupling constant varies when the detuning changes. To distinguish this case ( $\varphi = 0$  and  $\delta > 0$ ) from the previous case ( $\varphi = \pi$  and  $\delta < 0$ ), we replace the previous notation  $\Omega$ ,  $\delta$ , and  $g$  by  $\Omega'$ ,  $\delta'$ , and  $g'$ , respectively [see Fig. 2(b)]. For simplicity, we use the same symbols  $\omega$ ,  $\omega_0$ , and  $\omega_c$  for the pulse frequency, the qubit transition frequency, and the cavity mode frequency [Fig. 2(b)].

Suppose now that qubit 1 is largely detuned (decoupled) from both the cavity mode and the pulse. This can be achieved by adjusting the level spacing of qubit 1 (this tunability of energy levels can be achieved in different types of qubits, e.g., solid-state qubits [15-20]), or by moving qubit 1 out of the cavity mode (e.g., trapped atoms [35,36]). Thus, after dropping the terms related to qubit 1 (i.e., the terms corresponding to the index  $j = 1$ ) from the collective operators  $S_+ = \sum_{j=1}^{n+1} \sigma_j^+$  and  $S_- = \sum_{j=1}^{n+1} \sigma_j^-$  involved in Hamiltonians (8) and (9), and replacing  $\Omega$ ,  $\delta$ , and  $g$  (for the case of  $\varphi = \pi$  and  $\delta < 0$ ) with  $\Omega'$ ,  $\delta'$ , and  $g'$  (for the case of  $\varphi = 0$  and  $\delta > 0$ ), we obtain from the Hamiltonians (8) and (9) (assuming  $\omega = \omega_0$ )

$$H'_1 = \frac{\Omega'}{2} (e^{i\varphi} S'_- + e^{-i\varphi} S'_+), \tag{20}$$

$$H'_2 = g' (e^{i\delta't} a S'_+ + e^{-i\delta't} a^\dagger S'_-), \tag{21}$$

which are written in the interaction picture with respect to  $H'_0 = -\frac{\omega_0}{2}S'_z + \omega_c a^\dagger a$ . Here,  $S'_z$ ,  $S'_-$ , and  $S'_+$  are the collective operators for the  $n$  qubits ( $2, 3, \dots, n+1$ ), which are given by

$$S'_z = \sum_{j=2}^{n+1} \sigma_{z,j}, \quad S'_- = \sum_{j=2}^{n+1} \sigma_j^-, \quad S'_+ = \sum_{j=2}^{n+1} \sigma_j^+. \quad (22)$$

In addition, the detuning  $\delta'$  is

$$\delta' = \omega_0 - \omega_c > 0. \quad (23)$$

When choosing  $\varphi = 0$ , the Hamiltonian (20) reduces to

$$H'_1 = \frac{\Omega'}{2} S'_x, \quad (24)$$

where

$$S'_x = S'_- + S'_+ = \sum_{j=2}^{n+1} \sigma_{x,j}. \quad (25)$$

Note that the Hamiltonian (24) has a form similar to Eq. (11) and that the Hamiltonian (21) has a form similar to Eq. (9). Therefore, it is straightforward to show that under the condition  $\Omega' \gg \delta'$ ,  $g'$ , when  $t = \tau' = 2\pi/\delta'$ , the evolution operator of the qubits (in the interaction picture with respect to  $H'_0$ ) is

$$U'(\tau') = \exp(-i\Omega'\tau'S'_x/2) \exp(-i\lambda'\tau'S'^2_x), \quad (26)$$

where  $\lambda' = g'^2/(4\delta') > 0$ . The evolution operator  $U'$  in Eq. (26) will be needed for the second step of operation for either one of the two alternative approaches (presented in section IV below) for the NTCP gate realization.

One can see that the operator described by Eq. (19) or Eq. (26) does not include the photon operator  $a$  or  $a^\dagger$  of the cavity mode. Therefore, *the cavity mode can be initially in an arbitrary state (e.g., in a vacuum state, a Fock state, a coherent state, or even a thermal state).*

In the following operation, we will also need the resonant interaction between qubits and the pulses. Suppose that the Rabi frequency for the pulse applied to qubit 1 is  $\Omega_1$  while the Rabi frequency for the pulses applied to qubits ( $2, 3, \dots, n+1$ ) is  $\Omega_r$ . The initial phase for each pulse is  $\varphi = 0$ . In the interaction picture with respect to  $\tilde{H}_0 = -\frac{\omega_0}{2}S_z$ , the interaction Hamiltonian for the qubit system and the pulses is thus given by

$$H_1 = \frac{\Omega_1}{2} \sigma_{x,1} + \frac{\Omega_r}{2} S'_x. \quad (27)$$

For an evolution time  $\tau$ , the time evolution operator for the Hamiltonian (27) is

$$\tilde{U}(\tau) = \exp[-i\Omega_1\tau\sigma_{x,1}/2] \exp[-i\Omega_r\tau S'_x/2]. \quad (28)$$

#### IV. IMPLEMENTATION OF THE NTCP GATE

The goal of this section is to demonstrate how the NTCP gate can be realized based on the unitary operators (19) and (26) obtained above. We will present two alternative methods for the gate implementation: one method based on the adjustment of the qubit transition frequency and another method which works mainly via the adjustment of the cavity mode frequency. We present these two alternative methods because some experimental implementations might find it easier to tune the qubit frequency  $\omega_0$  while others will prefer to tune the cavity frequency  $\omega_c$ .

##### A. First method

Let us consider  $(n+1)$  qubits placed in a single-mode cavity or coupled to a resonator. For this first method, the cavity mode frequency  $\omega_c$  is kept fixed. The operations for the gate implementation, and the unitary evolutions after each step of operation, are listed below:

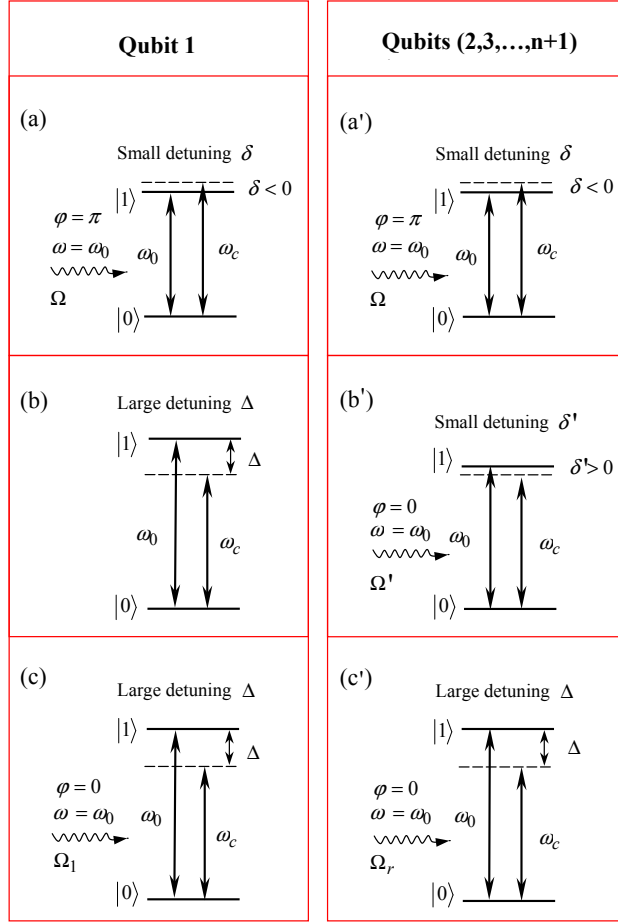


FIG. 3: Change of the qubit transition frequency  $\omega_0$  (or the qubit level spacings) of each qubit during a three-step NTCP gate. The three figures on the left side corresponds to the control qubit 1 while the three figures on the right side corresponds to each of the target qubits (2, 3, ...,  $n + 1$ ). Figures (a) and (a'), figures (b) and (b'), and figures (c) and (c') correspond to the operations of step (i), step (ii), and step (iii), respectively. In each figure, the two horizontal solid lines represent the qubit energy levels for the states  $|0\rangle$  and  $|1\rangle$ ;  $\omega_0$  is the qubit  $|0\rangle \leftrightarrow |1\rangle$  transition frequency;  $\omega_c$  is the cavity mode frequency;  $\omega$  is the pulse frequency;  $\varphi$  is the initial phase of the pulse; and either  $\Omega$ ,  $\Omega'$ ,  $\Omega_1$ , or  $\Omega_r$  is the Rabi frequency of the pulse. In addition,  $\delta$  and  $\delta'$  are the small detunings of the cavity mode with the  $|0\rangle \leftrightarrow |1\rangle$  transition, which are given by  $\delta = \omega_0 - \omega_c < 0$  and  $\delta' = \omega_0 - \omega_c > 0$ ; while  $\Delta = \omega_0 - \omega_c$  represents the large detuning of the cavity mode with the  $|0\rangle \leftrightarrow |1\rangle$  transition. Note that the cavity mode frequency  $\omega_c$  is kept fixed during the entire process, but the qubit transition frequency  $\omega_0$  is adjusted to achieve a different detuning  $\delta$ ,  $\delta'$ , or  $\Delta$ . Because the same detuning is set for each of the target qubits (2, 3, ...,  $n + 1$ ) for each of the three steps [see (a'), (b'), and (c')], the level spacings for the target qubits (2, 3, ...,  $n + 1$ ) can be synchronously adjusted (e.g., doable for solid-state qubits), by changing the common external parameters.

Step (i): Apply a resonant pulse (with  $\varphi = \pi$ ) to each qubit. The pulse Rabi frequency is  $\Omega$ . The cavity mode is coupled to each qubit with a detuning  $\delta < 0$  [Fig. 3(a) and Fig. 3(a')]. This is the case discussed in subsection III. A. Thus, the  $U$  in Eq. (19) is the evolution operator for the qubit system for an interaction time  $\tau = -2\pi/\delta$ .

Step (ii): Adjust the qubit transition frequency for qubits (2, 3, ...,  $n + 1$ ), such that the cavity mode is coupled to qubits (2, 3, ...,  $n + 1$ ) with a detuning  $\delta' > 0$  [Fig. 3(b')]. Apply a resonant pulse (with  $\varphi = 0$ ) to each of the target qubits (2, 3, ...,  $n + 1$ ) [Fig. 3(b')]. The pulse Rabi frequency is now  $\Omega'$ . In addition, adjust the transition frequency of qubit 1 such that qubit 1 is decoupled from the cavity mode and the pulses applied to qubits (2, 3, ...,  $n + 1$ ) [Fig. 3(b)]. It can be seen that this is the case discussed in subsection III. B. Thus, the  $U'$  of Eq. (26) is the evolution operator for the qubit system for an interaction time  $\tau' = 2\pi/\delta'$ .

The combined time evolution operator, after the above two steps, is

$$\begin{aligned}
 U(\tau + \tau') &= U'(\tau') U(\tau) \\
 &= e^{-i\Omega'\tau' S'_x/2} e^{-i\lambda'\tau' S'^2_x} e^{i\Omega\tau S_x/2} e^{i\lambda\tau S_x^2} \\
 &= \exp[i\Omega\tau (S_x - S'_x)/2] \exp[i\lambda\tau (S_x^2 - S'^2_x)].
 \end{aligned} \tag{29}$$

In the last line of Eq. (29), we assumed  $\Omega\tau = \Omega'\tau'$  (i.e.,  $-\Omega/\delta = \Omega'/\delta'$ ) and  $\lambda\tau = \lambda'\tau'$  (i.e.,  $-g/\delta = g'/\delta'$ ), which can be easily achieved by adjusting the detunings  $\delta$  and  $\delta'$  (i.e., changing the qubit transition frequency) as well as the Rabi frequencies  $\Omega$  and  $\Omega'$  (i.e., changing the intensity/amplitude of the pulses). Note that  $S_x - S'_x = \sigma_{x,1}$  and  $S_x^2 - S'^2_x = I + 2\sigma_{x,1}S'_x$ , where  $I$  is the identity operator for qubit 1. Thus, Eq. (29) can be written as

$$U(\tau + \tau') = \exp[i\Omega\tau\sigma_{x,1}/2] \exp[i2\lambda\tau\sigma_{x,1}S'_x]. \quad (30)$$

Step: (iii) Leave the transition frequency unchanged for qubit 1 [Fig. 3(c)] but adjust the transition frequency of qubits  $(2, 3, \dots, n+1)$  [Fig. 3(c')], such that the cavity mode is largely detuned (decoupled) from each qubit. In addition, apply a resonant pulse (with  $\varphi = 0$ ) to each qubit. The Rabi frequency for the pulse applied to qubit 1 is now  $\Omega_1$  [Fig. 3(c)] while the Rabi frequency of the pulse applied to qubits  $(2, 3, \dots, n+1)$  is  $\Omega_r$  [Fig. 3(c')]. In this case, the interaction Hamiltonian for the qubit system and the pulses is given by Eq. (27) and thus the time evolution operator is the  $\tilde{U}$  in Eq. (28) for an evolution time  $\tau$  given above.

It can be seen that after the above three-step operation, the joint time-evolution operator of the qubit system is

$$\begin{aligned} U(2\tau + \tau') &= \tilde{U}(\tau) U(\tau + \tau') \\ &= e^{-i(\Omega_1 - \Omega)\tau\sigma_{x,1}/2} e^{-i\Omega_r\tau S'_x/2} e^{i2\lambda\tau\sigma_{x,1}S'_x}. \end{aligned} \quad (31)$$

Under the following condition

$$\begin{aligned} \Omega_1 &= 4\lambda n + \Omega = -ng^2/\delta + \Omega, \\ \Omega_r &= 4\lambda = -g^2/\delta \end{aligned} \quad (32)$$

(which can be easily obtained by adjusting the Rabi frequencies  $\Omega$ ,  $\Omega_1$  and  $\Omega_r$ ), Eq. (31) can be then written as

$$U(2\tau + \tau') = \prod_{j=2}^{n+1} U_p(1, j) \quad (33)$$

with

$$U_p(1, j) = \exp[-i2\lambda\tau(\sigma_{x,1} + \sigma_{x,j} - \sigma_{x,1}\sigma_{x,j})]. \quad (34)$$

It can be easily shown that for the qubit pair  $(1, j)$ , we have

$$\begin{aligned} U_p(1, j) |\tilde{0}_1\rangle |\tilde{0}_j\rangle &= |\tilde{0}_1\rangle |\tilde{0}_j\rangle, \\ U_p(1, j) |\tilde{0}_1\rangle |\tilde{1}_j\rangle &= |\tilde{0}_1\rangle |\tilde{1}_j\rangle, \\ U_p(1, j) |\tilde{1}_1\rangle |\tilde{0}_j\rangle &= |\tilde{1}_1\rangle |\tilde{0}_j\rangle, \\ U_p(1, j) |\tilde{1}_1\rangle |\tilde{1}_j\rangle &= \exp(i8\lambda\tau) |\tilde{1}_1\rangle |\tilde{1}_j\rangle, \end{aligned} \quad (35)$$

where an overall phase factor  $\exp(-i2\lambda\tau)$  is omitted. Here and below,  $|\tilde{0}_1\rangle = (|0_1\rangle + |1_1\rangle)/\sqrt{2}$ , and  $|\tilde{1}_1\rangle = (|0_1\rangle - |1_1\rangle)/\sqrt{2}$ , are the two eigenstates of the Pauli operator  $\sigma_{x,1}$  for qubit 1; while  $|\tilde{0}_j\rangle = (|0_j\rangle + |1_j\rangle)/\sqrt{2}$ , and  $|\tilde{1}_j\rangle = (|0_j\rangle - |1_j\rangle)/\sqrt{2}$ , are the two eigenstates of the Pauli operator  $\sigma_{x,j}$  for qubit  $j$  ( $j = 2, 3, \dots$ , or  $n+1$ ). By setting  $8\lambda\tau = (2k+1)\pi$ , i.e.,

$$4g^2/\delta^2 = 2k+1 \quad (36)$$

( $k$  is an integer), we obtain from Eq. (35)

$$\begin{aligned} U_p(1, j) |\tilde{0}_1\rangle |\tilde{0}_j\rangle &= |\tilde{0}_1\rangle |\tilde{0}_j\rangle, \\ U_p(1, j) |\tilde{0}_1\rangle |\tilde{1}_j\rangle &= |\tilde{0}_1\rangle |\tilde{1}_j\rangle, \\ U_p(1, j) |\tilde{1}_1\rangle |\tilde{0}_j\rangle &= |\tilde{1}_1\rangle |\tilde{0}_j\rangle, \\ U_p(1, j) |\tilde{1}_1\rangle |\tilde{1}_j\rangle &= -|\tilde{1}_1\rangle |\tilde{1}_j\rangle, \end{aligned} \quad (37)$$



which shows that a quantum phase gate described by

$$U_p(1, j) = I_j - 2 \left| \tilde{1}_1 \tilde{1}_j \right\rangle \left\langle \tilde{1}_1 \tilde{1}_j \right|, \quad (38)$$

is achieved for the qubit pair  $(1, j)$ . Here,  $I_j$  is the identity operator for the qubit pair  $(1, j)$ , which is given by  $I_j = \sum_{kl} |k_1 l_j\rangle \langle k_1 l_j|$  with  $k, l \in \{\tilde{0}, \tilde{1}\}$ . Note that the condition (36) can be achieved by adjusting the detuning  $\delta$  (i.e., via changing the qubit transition frequency  $\omega_0$ ).

Combining Eqs. (33) and (38), we finally have

$$U(2\tau + \tau') = \prod_{j=2}^{n+1} \left( I_j - 2 \left| \tilde{1}_1 \tilde{1}_j \right\rangle \left\langle \tilde{1}_1 \tilde{1}_j \right| \right), \quad (39)$$

which demonstrates that  $n$  two-qubit CP gates are simultaneously performed on the qubit pairs  $(1, 2)$ ,  $(1, 3)$ , ..., and  $(1, n+1)$ , respectively. Note that each qubit pair contains the *same* control qubit (qubit 1) and a *different* target qubit (either qubit 2, 3, ..., or  $n+1$ ). Hence, a NTCP gate with  $n$  target qubits  $(2, 3, \dots, n+1)$  and one control qubit (qubit 1) is obtained after the above three-step process.

From the description above, one can see that the method presented here has an advantage: *it does not require the adjustment of the cavity-mode frequency*. For solid state qubits such as superconducting qubits and semiconductor quantum dots, the qubit transition frequency (or the qubit level spacings) can be readily adjusted by varying the external parameters (e.g., the external magnetic flux for superconducting charge qubits, the flux bias or current bias in the case of superconducting phase qubits and flux qubits, see e.g. [15-19], and the external electric field for semiconductor quantum dots [20]).

Before ending this subsection, it should be mentioned that since the detuning is set to be identical for each of the target qubits  $(2, 3, \dots, n+1)$  for each of the above steps [see Fig. 3(a', b', c')], the level spacings for the target qubits  $(2, 3, \dots, n+1)$  can be *synchronously* adjusted (e.g., doable for solid-state qubits), by changing the common external parameters. For instance, for superconducting charge qubits, this can be achieved by simultaneously changing the magnetic flux  $\Phi$  applied to the SQUID loop of each charge qubit via varying the common external electric current  $I$  (see Fig. 7 below).

As shown above, when qubits are placed in a cavity or coupled to a resonator during the entire operation (this applies to solid state qubits which are usually built in a cavity or resonator), tuning the transition frequency  $\omega_0$  of qubit 1 for step (ii) is needed to achieve a large detuning  $\Delta$  such that qubit 1 is decoupled from the cavity mode during steps (ii) and (iii) [Fig. 3(b, c)]. The same applies to qubits  $(2, 3, \dots, n+1)$  for step (iii) [Fig. 3(c')]. However, it should be noted that for trapped atoms, decoupling of qubits with the cavity mode can be made by moving atoms out of the cavity. When qubits are atoms, one can move qubit 1 out of the cavity for steps (ii) and (iii) to have this qubit decoupled from the cavity. Therefore, no adjustment of the transition frequency  $\omega_0$  is required for qubit 1 during the entire operation. Note that in the same manner, qubits  $(2, 3, \dots, n+1)$  (atoms) can be decoupled from the cavity for step (iii) and thus no adjustment of the transition frequency  $\omega_0$  (or the level spacings) of qubits  $(2, 3, \dots, n+1)$  is needed for this step (iii).

## B. Second method

In this subsection, we present a different way for realizing the NTCP gate, which is mainly based on the adjustment of the cavity mode frequency  $\omega_c$ . The cavity mode frequency  $\omega_c$  can be changed in various experiments (e.g., [21-25]).

Let us consider  $(n+1)$  qubits placed in a single-mode cavity or coupled to a resonator. Note that now the transition frequency  $\omega_0$  of the  $n$  target qubits  $(2, 3, \dots, n+1)$  is kept fixed during the following entire process. The operations for the gate implementation and the unitary evolutions after each step are listed below:

Step (i): Apply a resonant pulse (with  $\varphi = \pi$ ) to each qubit. The pulse Rabi frequency is  $\Omega$ . The cavity mode is coupled to each qubit with a detuning  $\delta < 0$  [Fig. 4(a) and Fig. 4(a')]. It can be seen that this is the case discussed in subsection III. A. Thus, the  $U$  of Eq. (19) is the evolution operator for the qubit system for an interaction time  $\tau = -2\pi/\delta$ .

Step (ii): Leave the transition frequency  $\omega_0$  of qubits  $(2, 3, \dots, n+1)$  unchanged while adjusting the cavity mode frequency  $\omega_c$ . The cavity mode is coupled to qubits  $(2, 3, \dots, n+1)$  with a detuning  $\delta' > 0$  [Fig. 4(b')]. Apply a resonant pulse (with  $\varphi = 0$ ) to each of qubits  $(2, 3, \dots, n+1)$  [Fig. 4(b')]. The pulse Rabi frequency is now  $\Omega'$ . In addition, adjust the transition frequency of qubit 1, such that qubit 1 is largely detuned (decoupled) from the cavity mode as well as the pulses applied to qubits  $(2, 3, \dots, n+1)$  [Fig. 4(b)]. One can see that this is the case discussed

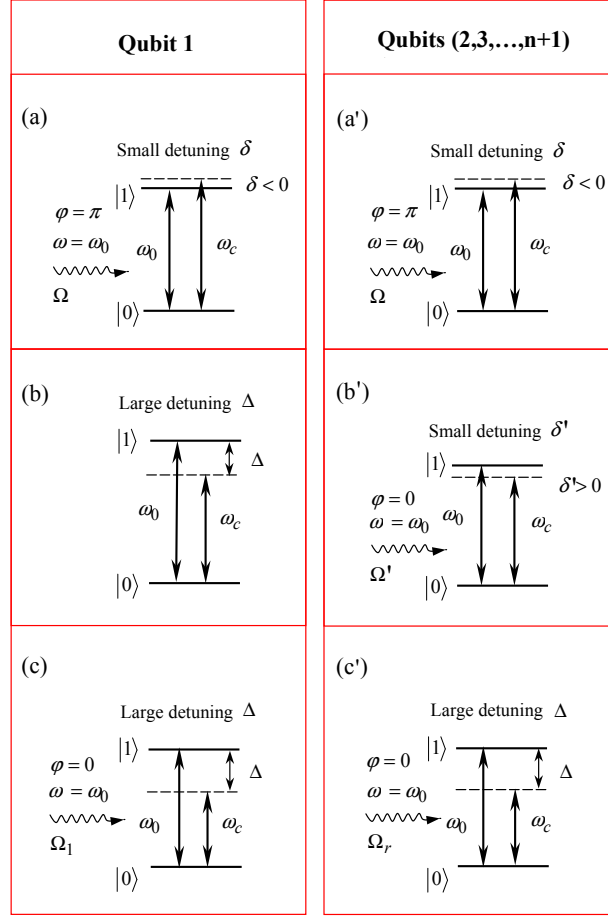


FIG. 4: Change of the cavity mode frequency  $\omega_c$  and the transition frequency  $\omega_0$  (or the level spacings) of qubit 1 during a three-step NTCP gate. This second method is an alternative way to implement the NTCP gate, which is different from the steps shown in Fig. 3. Note that the transition frequency  $\omega_0$  for qubits  $(2, 3, \dots, n+1)$  remains unchanged during this method. The three figures on the left side correspond to the control qubit 1, which (from top to bottom) are for the operations of step (i), step (ii), and step (iii), respectively. The three figures on the right side correspond to each of the qubits  $(2, 3, \dots, n+1)$ , which (from top to bottom) are respectively for the operations of step (i), step (ii), and step (iii). In each figure, the two horizontal solid lines represent the qubit levels  $|0\rangle$  and  $|1\rangle$ ;  $\omega_0$  is the qubit transition frequency;  $\omega_c$  is the cavity mode frequency;  $\omega$  is the pulse frequency;  $\varphi$  is the initial phase of the pulse; and either  $\Omega$ ,  $\Omega'$ ,  $\Omega_1$ , or  $\Omega_r$  is the Rabi frequency of the pulse (for various steps). In addition,  $\delta$  and  $\delta'$  are the small detunings of the cavity mode with the  $|0\rangle \leftrightarrow |1\rangle$  transition, which are given by  $\delta = \omega_0 - \omega_c < 0$  and  $\delta' = \omega_0 - \omega_c > 0$ ; while  $\Delta = \omega_0 - \omega_c$  represents the large detuning of the cavity mode with the  $|0\rangle \leftrightarrow |1\rangle$  transition.

in subsection III. B. Hence, the  $U'$  of Eq. (26) is the evolution operator for the qubit system for an interaction time  $\tau' = 2\pi/\delta'$ .

Step (iii): Leave the transition frequency  $\omega_0$  of qubits  $(2, 3, \dots, n+1)$  unchanged while adjusting the transition frequency of the control qubit 1 back to its original setting in step (i) [Fig. 4(c)]. Adjust the cavity mode frequency  $\omega_c$ , such that the cavity mode is largely detuned (decoupled) from each qubit [Fig. 4(c) and Fig. 4(c')]. In addition, apply a resonant pulse (with  $\varphi = 0$ ) to each qubit. The Rabi frequency for the pulse applied to qubit 1 is now  $\Omega_1$  [Fig. 4(c)] while the Rabi frequency of the pulses applied to qubits  $(2, 3, \dots, n+1)$  is now  $\Omega_r$  [Fig. 4(c')]. Therefore, the interaction Hamiltonian for the qubits and the pulses is  $H_1$  in Eq. (27) and thus the time evolution operator is the  $\tilde{U}$  in Eq. (28) for an evolution time  $\tau$  given above.

Note that the time evolution operators  $U$ ,  $U'$ , and  $\tilde{U}$ , obtained from each step discussed in this subsection, are the same as those obtained from each step of operations in the previous subsection. Hence, it is clear that the NTCP gate can be implemented after this three-step process.

From the description above, it can be seen that the transition frequency  $\omega_0$  for each one of the  $n$  target qubits  $(2, 3, \dots, n+1)$  remains unchanged during the entire operation. Thus, adjusting the level spacings for the  $n$  target qubits  $(2, 3, \dots, n+1)$  is *not* required by the method presented in this subsection. What one needs to do is to adjust

the cavity mode frequency and the level spacings of the control qubit 1 (*only one qubit*).

Before ending this subsection, it should be mentioned that for trapped atoms, decoupling of qubit 1 with the cavity mode for steps (ii) and (iii) as well as decoupling of qubits  $(2, 3, \dots, n+1)$  with the cavity mode for step (iii) can be achieved by moving atoms out of the cavity [35,36]. Therefore, when qubits are atoms, *no adjusting the qubit frequency (or the qubit level spacings) for all qubits is required during the entire operation and no adjustment of the cavity mode frequency is needed during step (iii)*. In Section VI, we will give a detailed discussion on how to extend this second method to implement the NTCP gate with trapped atoms, by moving the atoms in or out of the cavity.

### C. Discussion

Above, we have presented two alternative methods for implementing the NTCP gate. Note that (a) when coupled to a cavity (or resonator) mode and driven by a classical pulse, many physical qubit systems (such as atoms, quantum dots, and superconducting qubits) have the same type of interaction described by the Hamiltonian (3) or a Hamiltonian having a similar form to Eq. (3), from which the four Hamiltonians (8), (9), (20), and (21), i.e., the key elements for the proposed NTCP gate implementation, are available. Therefore, the two alternative methods above are quite general, which can be applied to implementing the NTCP gate with superconducting qubits, quantum dots, and trapped atomic qubits.

For the two approaches above, in Appendixes A and B, we provide guidelines on protecting qubits from leaking out of the computational subspace in the presence of more qubit levels. As discussed there, (a) as long as a large detuning  $\Delta_2$  of the cavity mode with the  $|1\rangle \leftrightarrow |2\rangle$  transition is satisfied, the leakage out of the computational subspace can be avoided for qubits belonging to case  $L$  (i.e., the case that the level spacing between the two levels  $|1\rangle$  and  $|2\rangle$  is larger than that between the levels  $|0\rangle$  and  $|1\rangle$ ); and (b) as long as a large detuning  $\Delta_2$  of the cavity mode with the  $|1\rangle \leftrightarrow |2\rangle$  transition as well as a large detuning  $\Delta_3$  of the cavity mode with the  $|1\rangle \leftrightarrow |3\rangle$  transition are met, the leakage out of the computational subspace can be suppressed for qubits belonging to case  $S$  (i.e., the case that the level spacing between the two levels  $|1\rangle$  and  $|2\rangle$  is smaller than that between the levels  $|0\rangle$  and  $|1\rangle$ ). Note that for either of the two methods above, the detuning is set to be identical for the target qubits  $(2, 3, \dots, n+1)$  for each of the three steps (Fig. 3(a', b', c') and Fig. 4(a', b', c')). Therefore, the level spacings of the  $n$  target qubits  $(2, 3, \dots, n+1)$  can be *synchronously* adjusted (e.g., doable for solid-state qubits), by changing the common external parameters. In this way, the gate implementation and the procedure for protecting qubits from the leakage can be greatly simplified because adjusting the level spacings of the  $n$  target qubits *one by one* would not be required.

We should mention that since the applied pulses are *resonant* with the  $|0\rangle \leftrightarrow |1\rangle$  transition, the coupling of the qubit level  $|0\rangle$  or  $|1\rangle$  with other levels, induced by the pulses, is negligibly small. Therefore, the leak out of the computation subspace, due to the application of the pulses, can be neglected. In addition, as shown above, the control qubit 1 needs to be decoupled from both of the cavity mode and the pulses applied to the target qubits  $(2, 3, \dots, n+1)$  during step (ii) for both of the two methods above. Note that during step (ii) for either of the two methods above, the detuning  $\delta'$  of the cavity mode with the  $|0\rangle \leftrightarrow |1\rangle$  transition of the target qubits  $(2, 3, \dots, n+1)$  is a small detuning [see Fig. 3(b') and Fig. 4(b')], and the pulses applied to the target qubits  $(2, 3, \dots, n+1)$  are resonant with the  $|0\rangle \leftrightarrow |1\rangle$  transition of the target qubits (i.e.,  $\omega = \omega_0$ ). Hence, for step (ii) of the two methods above, the control qubit 1 is also decoupled from the pulses applied to the target qubits  $(2, 3, \dots, n+1)$  when it is decoupled (large detuned) from the cavity mode.

It should be noted that for both of the two methods, the three steps presented above for the gate implementation, the Fig. 3 and Fig. 4, and the guidelines on protecting qubits from leakage presented in Appendixes A and B are for the case that: qubits are placed in a cavity or coupled to a resonator during the entire operation. This case particularly applies to solid state qubits because the positions of solid-state qubits such as superconducting qubits and quantum dots are fixed once they are built in a cavity or resonator. In this case, as shown above, adjustment of the qubit frequency  $\omega_0$  or the cavity frequency  $\omega_c$  is required in order to achieve a large detuning such that qubits are decoupled from the cavity mode. However, as mentioned above, for trapped atomic qubits, decoupling of qubits from the cavity can be made by just moving atoms out of the cavity and thus adjustment of the level spacings of atoms is not needed to have atoms decoupled (largely detuned) from the cavity mode (e.g., as shown in Section VI).

Finally, we should point out that when the leakage out of the computational subspace is not considered, other approaches for implementing the NTCP gate, which do not require adjusting the cavity mode frequency  $\omega_c$  or the qubit frequency  $\omega_0$ , are possible when the cavity or resonator is not initially in an arbitrary state (in other words, preparation of a specific initial state of the cavity or resonator would be needed).

Before closing this section, it should be mentioned that the present method is based on an effective Hamiltonian

$$H_{\text{eff}} = \sum_{j=2}^{n+1} H_{1j} = 2\lambda \sum_{j=2}^{n+1} (\sigma_{x,1} + \sigma_{x,j} - \sigma_{x,1}\sigma_{x,j}), \quad (40)$$

which can be found from Eqs. (33) and (34). One can see that this Hamiltonian contains the interaction terms between the control qubit (qubit 1) and each target qubit, but does not include the interaction terms between any two target qubits. Note that each term  $H_{1j}$  in Eq. (40) acts on a different target qubit, with the same control qubit, and that any two terms  $H_{1j}$  for different  $j$ 's commute with each other. Therefore, the  $n$  two-qubit controlled-phase gates forming the NTCP gate can be *simultaneously* performed on the qubit pairs (1, 2), (1, 3), ..., and (1,  $n + 1$ ), respectively.

## V. REALIZING THE NTCP GATE WITH SUPERCONDUCTING QUBITS COUPLED TO A RESONATOR

The method presented above for implementing the NTCP gate is based on the four Hamiltonians (8), (9), (20) and (21). In this section, we show how these Hamiltonians can be obtained for the superconducting charge qubits coupled to a resonator. We will then show how to apply the first method above to implement the NTCP gate with charge qubits coupled to a resonator. A discussion on the experimental feasibility will be given later.

### A. Hamiltonians

The superconducting charge qubit considered here, as shown in Fig. 5(a), consists of a small superconducting box with excess Cooper-pair charges, connected to a symmetric superconducting quantum interference device (SQUID) with capacitance  $C_{J0}$  and Josephson coupling energy  $E_{J0}$ . In the charge regime  $\Delta \gg E_c \gg E_{J0} \gg k_B T$  (here,  $k_B$ ,  $\Delta$ ,  $E_c$ , and  $T$  are the Boltzmann constant, gap, charging energy, and temperature, respectively), only two charge states,  $n = 0$  and  $n = 1$ , are important for the dynamics of the system, and thus this device [15-17] behaves as a two-level system. This superconducting two-level system can be represented by a spin-1/2 notation such that the charge states  $n = 0$  and  $n = 1$  correspond to eigenstates  $|\tilde{0}\rangle$  and  $|\tilde{1}\rangle$  of the spin operator  $\tilde{\sigma}_z$ , respectively. The Hamiltonian describing the qubit is thus given by [15,16]

$$H_q = -2E_c(1 - 2n_g)\tilde{\sigma}_z - E_J(\Phi)\tilde{\sigma}_x, \quad (41)$$

where  $n_g = C_g V_g / (2e)$ ,  $E_c = e^2 / (2C_g + 4C_{J0})$ ,  $E_J(\Phi) = 2E_{J0} \cos(\pi\Phi/\Phi_0)$ ,  $\tilde{\sigma}_z = |\tilde{0}\rangle\langle\tilde{0}| - |\tilde{1}\rangle\langle\tilde{1}|$  and  $\tilde{\sigma}_x = |\tilde{0}\rangle\langle\tilde{1}| + |\tilde{1}\rangle\langle\tilde{0}|$ . Here,  $C_g$  is the gate capacitance,  $V_g$  is the gate voltage,  $\Phi$  is the external magnetic flux applied to the SQUID loop,  $\Phi_0 = h/2e$  is the flux quantum, and  $E_J(\Phi)$  is the effective Josephson coupling energy. We assume that  $V_g = V_g^{\text{dc}} + V_g^{\text{ac}} + V_g^{\text{qu}}$ , where  $V_g^{\text{dc}}$  ( $V_g^{\text{ac}}$ ) is the dc (ac) part of the gate voltage and  $V_g^{\text{qu}}$  is the quantum part of the gate voltage, which is caused by the electric field of the resonator mode when the qubit is coupled to a resonator. Correspondingly, we have

$$n_g = n_g^{\text{dc}} + n_g^{\text{ac}} + n_g^{\text{qu}}, \quad (42)$$

where  $n_g^{\text{dc}} = C_g V_g^{\text{dc}} / (2e)$ ,  $n_g^{\text{ac}} = C_g V_g^{\text{ac}} / (2e)$ , and  $n_g^{\text{qu}} = C_g V_g^{\text{qu}} / (2e)$ . By inserting Eq. (42) into Eq. (41), we obtain the following Hamiltonian for the qubit-cavity system

$$H = E_z \tilde{\sigma}_z - E_J(\Phi) \tilde{\sigma}_x + \hbar\omega_c a^\dagger a + 4E_c n_g^{\text{ac}} \tilde{\sigma}_z + 4E_c n_g^{\text{qu}} \tilde{\sigma}_z, \quad (43)$$

where  $E_z = -2E_c(1 - 2n_g^{\text{dc}})$ . When  $V_g^{\text{ac}} = V_0 \cos(\omega t + \varphi)$  and  $V_g^{\text{qu}} = V_0^{\text{qu}}(a + a^\dagger)$ , the Hamiltonian (43) becomes

$$H = E_z \tilde{\sigma}_z - E_J(\Phi) \tilde{\sigma}_x + \hbar\omega_c a^\dagger a + \hbar\Omega \cos(\omega t + \varphi) \tilde{\sigma}_z + \hbar g (a + a^\dagger) \tilde{\sigma}_z, \quad (44)$$

where  $\Omega = 2E_c C_g V_0 / (\hbar e)$  is the Rabi frequency of the ac gate voltage and  $g = 2E_c C_g V_0^{\text{qu}} / (\hbar e)$  is the coupling constant between the charge qubit and the resonator mode.

Let us now consider  $N$  identical charge qubits coupled to a single-mode resonator [Fig. 5(b)]. One can select a subset of qubits for the gate, while the remaining qubits, which are not controlled by the gate, are decoupled from the resonator mode by setting their  $\Phi = \Phi_0/2$ ,  $V_g^{\text{dc}} = e/C_g$ , and  $V_g^{\text{ac}} = 0$  to have their free Hamiltonian being zero. Without loss of generality, we assume that the set of qubits selected for the gate are the  $(n + 1)$  qubits labelled by 1, 2, ..., and  $n + 1$  (here,  $1 < n < N$ ). From the discussion above, it can be seen that the Hamiltonian for the  $(n + 1)$  qubits and the resonator mode is

$$H = \hbar\omega_c a^\dagger a + \left[ E_z \tilde{S}_z - E_J(\Phi) \tilde{S}_x + \hbar\Omega \cos(\omega t + \varphi) \tilde{S}_z + \hbar g (a + a^\dagger) \tilde{S}_z \right], \quad (45)$$

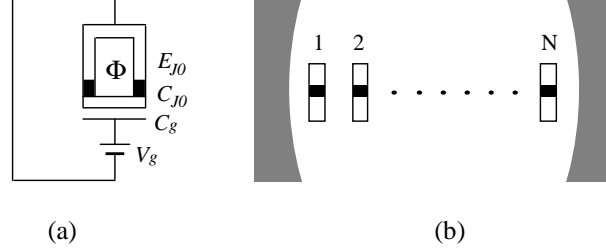


FIG. 5: (a) Schematic diagram of a superconducting charge qubit. (b)  $N$  superconducting qubits are placed in a microwave cavity (i.e., coupled to a resonator), from which a subset of qubits, selected for the gate, are coupled to each other via the resonator mode. The remaining qubits, which are not controlled by the gate, are decoupled from the resonator mode by setting their  $\Phi = \Phi_0/2$ ,  $V_g^{\text{dc}} = e/C_g$ , and  $V_g^{\text{ac}} = 0$  to have their free Hamiltonian being zero.

where  $\tilde{S}_z = \sum_{j=1}^{n+1} \tilde{\sigma}_{z,j}$  and  $\tilde{S}_x = \sum_{j=1}^{n+1} \tilde{\sigma}_{x,j}$ , with  $\tilde{\sigma}_{z,j} = |\tilde{0}_j\rangle\langle\tilde{0}_j| - |\tilde{1}_j\rangle\langle\tilde{1}_j|$  and  $\tilde{\sigma}_{x,j} = |\tilde{0}_j\rangle\langle\tilde{1}_j| + |\tilde{1}_j\rangle\langle\tilde{0}_j|$ . By setting  $E_z = 0$  (i.e.,  $n_g^{\text{dc}} = 1/2$ ) for each qubit and defining  $\omega_0/2 = E_J(\Phi)/\hbar$ , the Hamiltonian (45) reduces to (assuming  $\hbar = 1$ )

$$H = \omega_c a^\dagger a + \left[ -\frac{\omega_0}{2} \tilde{S}_z + \Omega \cos(\omega t + \varphi) \tilde{S}_x + g(a + a^\dagger) \tilde{S}_z \right]. \quad (46)$$

Define now the new qubit basis  $|\tilde{0}_j\rangle = (|\tilde{0}_j\rangle + |\tilde{1}_j\rangle)/\sqrt{2}$  and  $|\tilde{1}_j\rangle = (|\tilde{0}_j\rangle - |\tilde{1}_j\rangle)/\sqrt{2}$ . Thus, in this new basis, the Hamiltonian (46) becomes

$$H = H_0 + H_1 + H_2, \quad (47)$$

where

$$H_0 = -\frac{\omega_0}{2} S_z + \omega_c a^\dagger a, \quad (48)$$

$$H_1 = \Omega \cos(\omega t + \varphi) S_x, \quad (49)$$

$$H_2 = g(a + a^\dagger) S_x. \quad (50)$$

Here, the collective operators  $S_z$  and  $S_x$  are the same as those given in Eq. (7) and Eq. (12). In the interaction picture with respect to  $H_0$ , we obtain from Eqs. (49) and (50) (under the rotating-wave approximation and assuming  $\omega = \omega_0$ )

$$H_1 = \frac{\Omega}{2} (e^{i\varphi} S_- + e^{-i\varphi} S_+), \quad (51)$$

$$H_2 = g(e^{i\delta t} a S_+ + e^{-i\delta t} a^\dagger S_-), \quad (52)$$

where the collective operators  $S_-$  and  $S_+$  are the same as those given in Eq. (7), and  $\delta = \omega_0 - \omega_c < 0$ .

Note that  $\omega_0 = 4E_{J0} \cos(\pi\Phi/\Phi_0)/\hbar$ . Hence, the qubit transition frequency  $\omega_0$  can be adjusted by changing the external magnetic flux  $\Phi$  applied to the SQUID loop of the charge qubit. Note also that for  $n$  charge qubits ( $n \geq 2$ ), their transition frequency  $\omega_0$  can be synchronously adjusted by simultaneously changing the external magnetic flux  $\Phi$  applied to the SQUID loop of each charge qubit, e.g., via changing the common external electric current  $I$  (see Fig. 7).

We now turn off the ac gate voltage applied to the charge qubit 1 (i.e., setting  $V_g^{\text{ac}} = 0$  for the charge qubit 1) and adjust the transition frequency  $\omega_0$  of the charge qubit 1 to have qubit 1 decoupled (largely detuned) from the resonator mode. In this way, we can drop the terms corresponding to the index  $j = 1$  from the collective operators  $S_+ = \sum_{j=1}^{n+1} \sigma_j^+$  and  $S_- = \sum_{j=1}^{n+1} \sigma_j^-$  involved in Hamiltonians (51) and (52). In addition, adjust either of the transition frequency  $\omega_0$  of qubits (2, 3, ...,  $n+1$ ) and the resonator frequency  $\omega_c$  to achieve a detuning  $\delta' = \omega_0 - \omega_c > 0$ , and set an ac gate voltage  $V_g^{\text{ac}} = V_0' \cos(\omega t + \varphi)$  (with  $\omega = \omega_0$ ) for each of qubits (2, 3, ...,  $n+1$ ). The Rabi frequency  $\Omega'$  for each ac gate voltage (i.e., the pulse) is given by  $\Omega' = 2E_c C_g V_0' / (\hbar e)$ . After replacing  $\Omega$ ,  $\delta$ , and  $g$ , with  $\Omega'$ ,  $\delta'$ , and  $g'$ , respectively; we can obtain from Eqs. (51) and (52)

$$H_1' = \frac{\Omega'}{2} (e^{i\varphi} S_- + e^{-i\varphi} S_+), \quad (53)$$

$$H_2' = g' (e^{i\delta' t} a S_+ + e^{-i\delta' t} a^\dagger S_-), \quad (54)$$

which are written in the interaction picture with respect to  $H'_0 = -\frac{\omega_0}{2}S'_z + \omega_c a^\dagger a$ . Here, the collective operators  $S'_z$ ,  $S'_+$ , and  $S'_-$  are the same as those given in Eq. (22).

One can see that the four Hamiltonians (51-54) obtained here have the same forms as the Hamiltonians (8), (9), (20), and (21), respectively. Hence, the NTCP gate can be implemented with charge qubits coupled to a resonator. A more detailed discussion on this is given in the next subsection.

### B. NTCP gates with charge qubits coupled to a resonator

A number of groups have proposed how to perform two-qubit logic gates using superconducting qubits coupled to an inductance [37], a capacitor [38], an LC circuit [39], or a superconducting resonator/cavity (see [18] for flux qubits and [40,41] for charge qubits). These and other proposals could be useful to produce the building blocks of superconducting quantum computers. In addition, it is noted that there is a growing interest in the physical realization of multiqubit gates which are important in quantum information processing. Recently, several approaches for implementing a multiqubit gate with  $n$ -control qubits acting on one target qubit based on cavity QED or ion traps have been proposed [8,11-14]. However, we note that these proposals cannot be extended to implement a multi-qubit gate with one qubit simultaneously controlling  $n$  target qubits.

Following the first method introduced in the previous section, we now discuss how to implement the NTCP gate with  $(n+1)$  charge qubits (1, 2, ...,  $n+1$ ), coupled to a superconducting resonator. To begin with, it should be mentioned that: (a) for each step of the operations below, the dc gate voltage  $V_g^{\text{dc}}$  for each one of qubits (1, 2, ...,  $n+1$ ) is set by  $V_g^{\text{dc}} = e/C_g$ , such that  $E_z = 0$  for each qubit; and (b) the resonator mode frequency  $\omega_c$  is kept *fixed* during the entire operation. The operations for the gate realization and the unitary evolutions after each step are given below:

Step (i): Set  $V_g^{\text{ac}} = V_0 \cos(\omega t + \pi)$  (with  $\varphi = \pi$ ) for each qubit. Here, the ac gate voltage frequency  $\omega$  is equal to the transition frequency  $\omega_0$  of each qubit. Each qubit is coupled to the resonator mode with a detuning  $\delta < 0$  [Fig. 6(a) and Fig. 6(a')]. In this case, as shown above, we have the Hamiltonian (51) for  $\varphi = \pi$  and the Hamiltonian (52), which take the same forms of the Hamiltonian (8) for  $\varphi = \pi$  and the Hamiltonian (9), respectively. One can see that this is the case discussed in subsection III. A. Thus, the time evolution operator for the qubit system corresponding to this step would be the  $U$  of Eq. (19) for an interaction time  $\tau = -2\pi/\delta$ .

Step (ii): Set  $V_g^{\text{ac}} = 0$  for qubit 1 and adjust the transition frequency  $\omega_0$  of qubit 1 to have qubit 1 decoupled from the resonator mode [Fig. 6(b)]. For qubits (2, 3, ...,  $n+1$ ), adjust their transition frequency  $\omega_0$  such that they are coupled to the resonator mode with a detuning  $\delta' > 0$  [Fig. 6(b')]. In addition, set  $V_g^{\text{ac}} = V'_0 \cos(\omega t)$  (with  $\varphi = 0$ ) for each of the target qubits (2, 3, ...,  $n+1$ ) [Fig. 6(b')]. Here, the ac gate voltage frequency  $\omega$  is equal to the transition frequency  $\omega_0$  of qubits (2, 3, ...,  $n+1$ ) [Fig. 6(b')]. According to the discussion above, we have the Hamiltonian (53) for  $\varphi = 0$  and the Hamiltonian (54), which take the same forms of the Hamiltonian (20) for  $\varphi = 0$  and the Hamiltonian (21), respectively. Hence, this is the case discussed in subsection III. B. The time evolution operator for the qubit system corresponding to this step would be the  $U'$  of Eq. (26) for an interaction time  $\tau' = 2\pi/\delta'$ .

Step (iii): Leave now the transition frequency  $\omega_0$  unchanged for qubit 1 while adjust the qubit transition frequency  $\omega_0$  for qubits (2, 3, ...,  $n+1$ ), such that each qubit is decoupled (largely detuned) from the resonator mode [Fig. 6(c) and Fig. 6(c')]. In addition, set  $V_g^{\text{ac}} = V_0^1 \cos(\omega t)$  for qubit 1 while  $V_g^{\text{ac}} = V'_0 \cos(\omega t)$  for each of qubits (2, 3, ...,  $n+1$ ), with  $\omega$  being equal to the transition frequency  $\omega_0$  of each qubit [Fig. 6(c) and Fig. 6(c')]. Thus, we can obtain the Hamiltonian  $H_1$  in Eq. (27), with  $\Omega_1 = 2E_c C_g V_0^1 / (\hbar e)$  and  $\Omega_r = 2E_c C_g V'_0 / (\hbar e)$ . Therefore, the unitary operator for this step is the  $\tilde{U}$  in Eq. (28) for an interaction time  $\tau$  given above.

From the description above, it can be seen that there is no need of adjusting the resonator mode frequency  $\omega_c$ . Hence, the procedure presented here for the gate realization is an extension of the first method introduced above (see subsection IV. A). Note that the three time-evolution operators  $U$ ,  $U'$ , and  $\tilde{U}$ , obtained from each step here, are the same as those obtained from each step in subsection IV. A. Therefore, following the same discussion given there, one can easily see that the NTCP gate can be implemented with  $(n+1)$  charge qubits (i.e., the *control* charge qubit 1 as well as the  $n$  *target* charge qubits 2, 3, ..., and  $n+1$ ). Namely, after the above three-step process, a phase flip (i.e.,  $|\tilde{1}\rangle \rightarrow -|\tilde{1}\rangle$ ) on the state  $|\tilde{1}\rangle$  of each *target* charge qubit is achieved when the *control* charge qubit 1 is initially in the state  $|\tilde{1}\rangle$ , but nothing happens to the states  $|\tilde{0}\rangle$  and  $|\tilde{1}\rangle$  of each *target* charge qubit when the *control* charge qubit 1 is initially in the state  $|\tilde{0}\rangle$ .

According to the discussion in subsection IV. A, it can be found that to implement the NTCP gate, the following conditions need to be satisfied: (a)  $\Omega \gg g, \delta$  and  $\Omega' \gg g', \delta'$ ; (b)  $\Omega_1 = -ng^2/\delta + \Omega$  and  $\Omega_r = -g^2/\delta$ ; (c)  $-\Omega/\delta = \Omega'/\delta'$  and  $-g/\delta = g'/\delta'$ ; and (d)  $4g^2/\delta^2 = 2k+1$ . These conditions can in principle be realized since: (i) The Rabi frequencies  $\Omega(V_0)$ ,  $\Omega'(V'_0)$ ,  $\Omega_1(V_0^1)$ , and  $\Omega_r(V'_0)$  are respectively the functions of the amplitudes  $V_0$ ,  $V'_0$ ,  $V_0^1$ , and  $V'_0$  of the ac

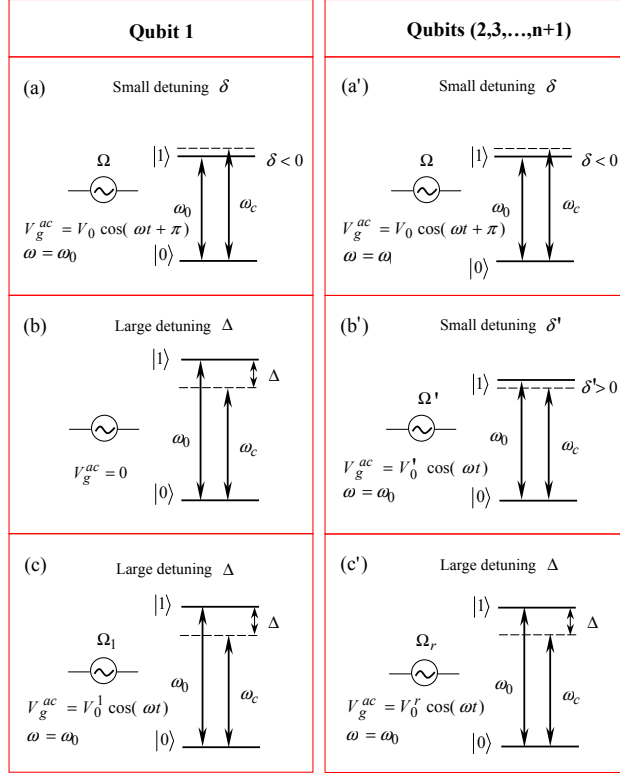


FIG. 6: Change of the qubit transition frequency  $\omega_0$  and the ac gate-voltage frequency  $\omega$  during a three-step NTCP gate with charge qubits coupled to a resonator. The three figures on the left side correspond to the charge control qubit 1, which (from top to bottom) are for the operations of step (i), step (ii), and step (iii), respectively. The three figures on the right side correspond to the charge target qubits (2, 3, ...,  $n+1$ ), (from top to bottom) for the operations of step (i), step (ii), and step (iii), respectively. In each figure, the two horizontal solid lines represent the qubit levels  $|0\rangle$  and  $|1\rangle$ ;  $\omega_c$  is the resonator mode frequency;  $\omega_0$  is the qubit transition frequency;  $\omega$  is the frequency of the ac gate voltage  $V_g^{ac}$  (i.e., the pulse); and  $\Omega$  ( $V_0$ ),  $\Omega'$  ( $V_0'$ ),  $\Omega_1$  ( $V_0^1$ ), or  $\Omega_r$  ( $V_0^r$ ) is the function of the amplitude  $V_0$ ,  $V_0'$ ,  $V_0^1$ , or  $V_0^r$  of the ac gate voltage, which can be adjusted by changing the ac gate-voltage amplitude; and each circle with a symbol  $\sim$  represents an ac gate voltage. In (b), the ac gate voltage for qubit 1 is set to zero (i.e.,  $V_g^{ac} = 0$ ). In addition,  $\delta$  and  $\delta'$  are the small detunings of the resonator mode with the  $|0\rangle \leftrightarrow |1\rangle$  transition, which are given by  $\delta = \omega_0 - \omega_c < 0$  and  $\delta' = \omega_0 - \omega_c > 0$ ; while  $\Delta = \omega_0 - \omega_c$  represents the large detuning of the resonator mode with the  $|0\rangle \leftrightarrow |1\rangle$  transition. Note that the resonator mode frequency  $\omega_c$  is kept fixed during the entire operation, but the qubit transition frequency  $\omega_0$  is adjusted to achieve a different detuning  $\delta$ ,  $\delta'$ , or  $\Delta$ . Since the same detuning is set for each of the target qubits (2, 3, ...,  $n+1$ ) [see (a'), (b'), and (c')], the level spacings for the target qubits (2, 3, ...,  $n+1$ ) can be synchronously adjusted, by changing the common external parameters [e.g., the external electric current  $I$  (see Fig. 7)].

gate voltages, which can be easily adjusted by changing the amplitudes of the ac gate voltages; and (ii) The detunings  $\delta$  and  $\delta'$  can be adjusted by changing the qubit transition frequency  $\omega_0$ . As mentioned above, the qubit transition frequency  $\omega_0$  can be readily changed by varying the external magnetic flux  $\Phi$  applied to the SQUID loop.

From Fig. 6(a', b', c'), it can be seen that the same detuning is set for each of the target qubits (2, 3, ...,  $n+1$ ) for each of the above steps. Therefore, the level spacings for the target qubits (2, 3, ...,  $n+1$ ) can be synchronously adjusted, by changing the common external parameters (e.g., the external electric current  $I$ ) (see Fig. 7).

Before ending this section, we give some discussion on the deviation from the degeneracy point for each of the qubits (1, 2, ...,  $n+1$ ), during each step described above. We find that:

(a) For step (i), the deviation from the degeneracy point for each one of the qubits (1, 2, ...,  $n+1$ ) is

$$\varepsilon_0 = |n_g - 1/2| = \hbar(\Omega + g)/(4E_c); \quad (55)$$

(b) For step (ii), the deviation from the degeneracy point for qubits (2, 3, ...,  $n+1$ ) is

$$\varepsilon_1 = \hbar(\Omega' + g')/(4E_c), \quad (56)$$

note that the deviation from the degeneracy point for qubit 1 is smaller than  $\varepsilon_1$  since  $n_g^{ac} = 0$  for qubit 1; and

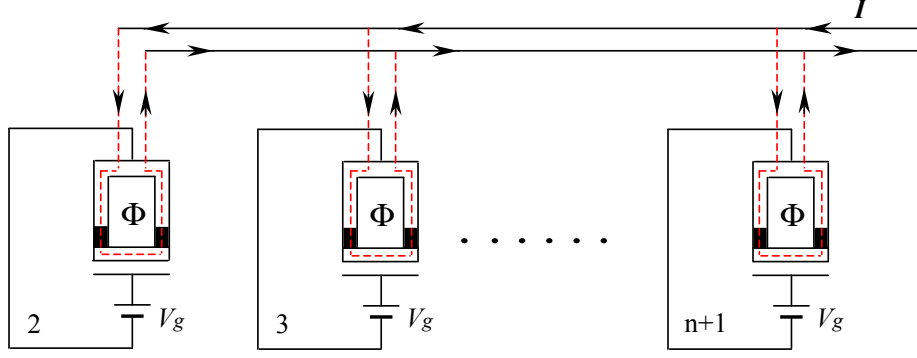


FIG. 7: An external flux  $\Phi$  is synchronously applied to  $n$  target charge qubits  $(2, 3, \dots, n+1)$ , which can be adjusted by changing the current  $I$ . Note that for flux-biased superconducting flux qubits or phase qubits, the qubit level spacings can be simultaneously adjusted in the same manner (e.g., by simultaneously changing the fluxes  $\Phi$  applied to SQUID loops via varying the common external current  $I$ ).

(d) For step (iii), the deviation from the degeneracy point for qubit 1 is

$$\varepsilon_2 \sim \hbar \Omega_1 / (4E_c), \quad (57)$$

and the deviation from the degeneracy point for qubits  $(2, 3, \dots, n+1)$  is

$$\varepsilon_3 \sim \hbar \Omega_r / (4E_c). \quad (58)$$

### C. Discussion

In this section we discuss some issues which are relevant for future experimental implementations of our proposal. For the methods to work: (a) The conditions for the Rabi frequencies  $\Omega$ ,  $\Omega'$ ,  $\Omega_1$ , and  $\Omega_r$ , which were discussed above, need to be met; (b) The total operation time

$$t_{\text{op}} = 2\tau + \tau' = 4\pi / |\delta| + 2\pi / \delta' \quad (59)$$

should be much shorter than the dephasing time  $T_2$  of the qubit (note that the energy relaxation time  $T_1$  is much longer than  $T_2$ ) and the lifetime of the resonator mode  $\kappa^{-1} = Q/\omega_c$ , where  $Q$  is the (loaded) quality factor of the resonator; (c) The deviation  $\varepsilon_0$ ,  $\varepsilon_1$ ,  $\varepsilon_2$ , and  $\varepsilon_3$  from the degeneracy point needs to be a small number to have the qubits working near the degeneracy point; and (d) The direct coupling between SQUIDs needs to be negligible, since this interaction is not intended. It is noted that the direct interaction between SQUIDs can be made negligibly small as long as  $D \gg d$  (where  $D$  is the distance between the two nearest SQUIDs and  $d$  is the linear dimension of each SQUID).

For the sake of definitiveness, let us consider the experimental feasibility of implementing a five-target-qubit controlled phase gate using superconducting charge qubits with parameters listed in Table 1. Note that charge qubits with these parameters are now readily available [42,43]. For a superconducting one dimensional standing-wave CPW (coplanar waveguide) resonator and each qubit placed at an antinode of the resonator mode (Fig. 8), the amplitude of the quantum part of the gate voltage is given by [44]

$$V_0^{\text{qu}} = (\hbar \omega_c)^{1/2} (L c_0)^{-1/2}, \quad (60)$$

where  $L$  is the length of the resonator and  $c_0$  is the capacitance per unit length of the resonator. Therefore, the coupling constant  $g$  is given by

$$g = 2E_c C_g (\hbar e)^{-1} (\hbar \omega_c)^{1/2} (L c_0)^{-1/2}, \quad (61)$$

showing that  $g$  does not depend on the detuning  $\delta$ . Therefore, we have  $g = g'$ , for which the above condition  $-\Omega/\delta = \Omega'/\delta'$  and  $-g/\delta = g'/\delta'$  simply turns to the  $\Omega = \Omega'$  and  $-\delta = \delta'$ . For the superconducting charge qubits with the parameters given in Table 1 and the resonator with the parameters listed in Table 2, a simple calculation gives  $g/2\pi \sim 22$  MHz, which is available in experiments (see, e.g., [45]). With a choice of  $-\delta = \delta' = 2g$  (corresponding



Charge qubit	
Gate capacitance	$C_g = 1 \text{ aF}$
Josephson capacitance	$C_{J0} = 300 \text{ aF}$
Charging energy	$E_c/h = 32 \text{ GHz}$
Josephson coupling energy	$E_{J0}/h = 5 \text{ GHz}$
Energy relaxation time	$T_1 = 7.3 \mu\text{s}$
Dephasing time	$T_2 = 500 \text{ ns}$

TABLE I: Possible experimental parameters of a charge qubit

Resonator	
Resonator frequency	$\omega_c/2\pi = 10 \text{ GHz}$
Wave length	$\lambda \sim 10 \text{ mm}$
Length of the resonator	$L = \lambda$
Capacitance per unit length of resonator	$c_0 \sim 0.22 \text{ aF}$
Effective relative dielectric constant	$\epsilon_e \sim 9$
Quality factor	$Q \sim 10^5$
Lifetime of the resonator mode	$\kappa^{-1} \sim 794 \text{ ns}$

TABLE II: Possible parameters of a resonator

to  $k = 0$ ), the total operation time  $t_{\text{op}}$  would be  $\sim 68 \text{ ns}$ , which is much shorter than the dephasing time  $T_2$  and  $\kappa^{-1} \sim 794 \text{ ns}$  for a resonator with  $Q = 10^5$ . Note that a superconducting CPW resonator with a quality factor of  $Q > 10^6$  has been experimentally demonstrated [46].

Based on  $\Omega = \Omega'$ ,  $\Omega_1 = 4\lambda n + \Omega$ , and  $\Omega_r = 4\lambda$  ( $n = 5$  for a five-target-qubit gate), we have  $\Omega'/(2\pi) \sim 440 \text{ MHz}$ ,  $\Omega_1/(2\pi) \sim 495 \text{ MHz}$ , and  $\Omega_r/(2\pi) \sim 11 \text{ MHz}$  for a choice of  $\Omega \sim 20g$ , i.e.,  $\Omega/(2\pi) \sim 440 \text{ MHz}$ . For the Rabi frequencies given here, we obtain  $\varepsilon_0 = \varepsilon_1 \sim 3.61 \times 10^{-3}$ ,  $\varepsilon_2 \sim 3.87 \times 10^{-3}$ , and  $\varepsilon_3 \sim 8.59 \times 10^{-5}$  for a qubit-cavity system with the parameters above. Therefore, the conditions for the qubits to work near the degeneracy point are well satisfied.

Finally, for a resonator with  $\omega_c/(2\pi) = 10 \text{ GHz}$ , the wavelength of the resonator mode is  $\lambda \sim 10 \text{ mm}$ . For the charge qubits placed in a resonator as shown in Fig. 8, the distance between any two nearest SQUIDs is  $D \sim \lambda/2 \sim 5 \text{ mm}$ . Hence, the ratio  $D/d$  would be  $\sim 250$  for  $d = 20 \mu\text{m}$ . Note that the dipole field generated by the current in each SQUID ring at a distance  $r \gg d$  decreases as  $r^{-3}$ . Thus, the condition of negligible direct coupling between SQUIDs is well satisfied.

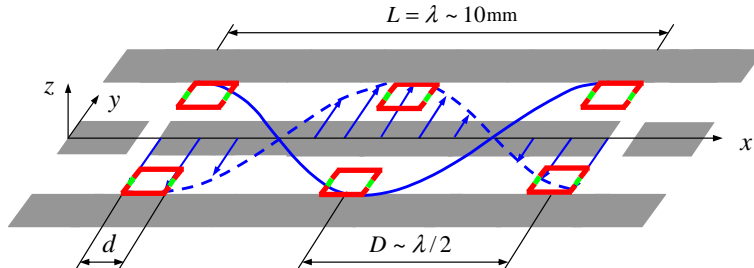


FIG. 8: (Color online) Proposed setup for six qubits (red squares) and a (grey) standing-wave quasi-one dimensional coplanar waveguide cavity (not drawn to scale). Each qubit is placed at an antinode of the electric field. The two blue curves represent the standing-wave electric field, along the  $y$ -direction;  $D$  is the distance between any two nearest SQUID loops; and  $d$  is the linear dimension of each SQUID loop.

Note that because of  $\omega_0 = 4E_{J0} \cos(\pi\Phi/\Phi_0)/\hbar$ , it can be found that for charge qubits with the parameters given in Table 1, the transition frequency  $\nu_0 = \omega_0/2\pi$  of each qubit varies from  $\nu_0 = 0$  GHz for  $\Phi/\Phi_0 = 1/2$  to  $\nu_0 = 20$  GHz for  $\Phi = 0$ . Therefore, the choice of the resonator frequency above is reasonable. For the choice of  $-\delta = \delta' = 2g$  above, the qubit transition frequency  $\nu_0$  would be  $\sim 9.956$  GHz for the detuning  $\delta = -2g$  while  $\sim 10.044$  GHz for the detuning  $\delta' = 2g$ .

The above analysis shows that the realization of a five-target-qubit controlled phase gate is possible using superconducting charge qubits and a resonator. We remark that a quantum-controlled phase gate with a larger number of target qubits can in principle be obtained by increasing the length of the resonator since the total operation time  $t_{\text{op}}$  is independent of the number of target qubits  $n$ .

The NTCP gate with charge qubits coupled to a resonator can be also implemented using the three steps of the second method introduced in the previous section. We emphasize that the primary purpose of this section is to provide an example to show how the proposal presented in the previous section can be applied to implement a NTCP gate with superconducting charge qubits coupled to a resonator. However, we note that (a) when coupled to a resonator mode and driven by classical pulses, superconducting flux or phase qubits have the same type of interaction described by the Hamiltonian (3) or a Hamiltonian having a similar form to Eq. (3), from which the above four Hamiltonians (8), (9), (20) and (21) can be achieved; and (b) the small detuning (i.e., the  $|0\rangle \leftrightarrow |1\rangle$  transition being nearly resonant with the resonator mode) and the large detuning (i.e., the transition between any two irrelevant levels is far off resonant with the resonator mode) can be obtained via the adjustment of the level spacings. Therefore, it is straightforward to show that the two alternative methods introduced in the previous section can be generalized to realize the NTCP gate with superconducting flux or phase qubits, by coupling them to a superconducting resonator.

## VI. NTCP GATE AND MULTI-QUBIT ENTANGLEMENT WITH ATOMS USING ONE CAVITY

In this section, we show how to extend the second method introduced in Section IV to realize a NTCP gate with two-level atoms, by the use of one cavity. We then give a discussion on how to prepare a multiqubit entangled state with atoms interacting with a cavity which is initially in an arbitrary state. Note that different from the procedure for the gate implementation given in subsection IV. B, decoupling of atoms with the cavity is based on moving the atoms out of the cavity.

### A. Realization of a NTCP gate with atoms

Consider  $(n+1)$  identical two-level atoms  $(1, 2, \dots, n+1)$ . The two levels of each atom are labelled by  $|0\rangle$  and  $|1\rangle$ . The transition frequency of each atom is denoted as  $\omega_0$ . Each atom is trapped in periodic potential of an one-dimensional optical lattice and can be loaded into or moved out of the cavity by translating the optical lattice [35,36]. We note that the NTCP gate can be realized as follows:

Step (i): Move atoms  $(1, 2, \dots, n+1)$  into the cavity and then apply a classical pulse (with an initial phase  $\varphi = \pi$  and a frequency  $\omega = \omega_0$ ) to the atoms [Fig. 9(a)]. The cavity mode is coupled to the  $|0\rangle \rightarrow |1\rangle$  transition of each atom, with a detuning  $\delta = \omega_0 - \omega_c < 0$ , which can be achieved by prior adjustment of the cavity mode frequency [21]. The Hamiltonian describing the atoms interacting with the pulses is  $H_1$  in Eq. (8) for  $\varphi = \pi$  while the Hamiltonian describing the atoms interacting with the cavity mode is  $H_2$  in Eq. (9). The time-evolution operator for this step is thus the  $U$  of Eq. (19) for an interaction time  $\tau = -2\pi/\delta$ .

Step (ii): Move atom 1 out of the cavity and then apply a classical pulse (with  $\varphi = 0$  and  $\omega = \omega_0$ ) to the atoms  $(2, 3, \dots, n+1)$  [Fig. 9(b)]. Adjust the cavity mode frequency such that the cavity mode is coupled to the  $|0\rangle \rightarrow |1\rangle$  transition of atoms  $(2, 3, \dots, n+1)$ , with a detuning  $\delta' = \omega_0 - \omega_c > 0$ . Since the atom 1 is now decoupled from the cavity mode, the Hamiltonian describing the atoms  $(2, 3, \dots, n+1)$  interacting with the pulses is thus  $H'_1$  in Eq. (20) for  $\varphi = 0$  while the Hamiltonian describing the atoms  $(2, 3, \dots, n+1)$  interacting with the cavity mode is  $H'_2$  in Eq. (21). The time-evolution operator for this step is thus the  $U'$  of Eq. (26) for an interaction time  $\tau' = 2\pi/\delta'$ .

Step (iii): Move atoms  $(2, 3, \dots, n+1)$  out of the cavity. Apply a classical pulse (with  $\varphi = 0$  and  $\omega = \omega_0$ ) to the control atom 1 and a classical pulse (with the same initial phase and frequency) to the target atoms  $(2, 3, \dots, n+1)$  [Fig. 9(c)]. The Rabi frequency for the pulse applied to atom 1 is  $\Omega_1$  while the Rabi frequency for the pulses applied to atoms  $(2, 3, \dots, n+1)$  is  $\Omega_r$ . The Hamiltonian describing the atoms  $(1, 2, \dots, n+1)$  interacting with the pulses is  $H_1$  in Eq. (27) and thus the time-evolution operator for this step is the  $\tilde{U}$  of Eq. (28) for an interaction time  $\tau$  given above.

Note that the three time-evolution operators  $U$ ,  $U'$ , and  $\tilde{U}$ , obtained from each step here, are the same as those obtained from each step in subsection IV. A. Therefore, as long as the conditions given in subsection IV. A are met, a NTCP gate described by Eq. (39) is implemented with the  $(n+1)$  atoms. Namely, after the above three

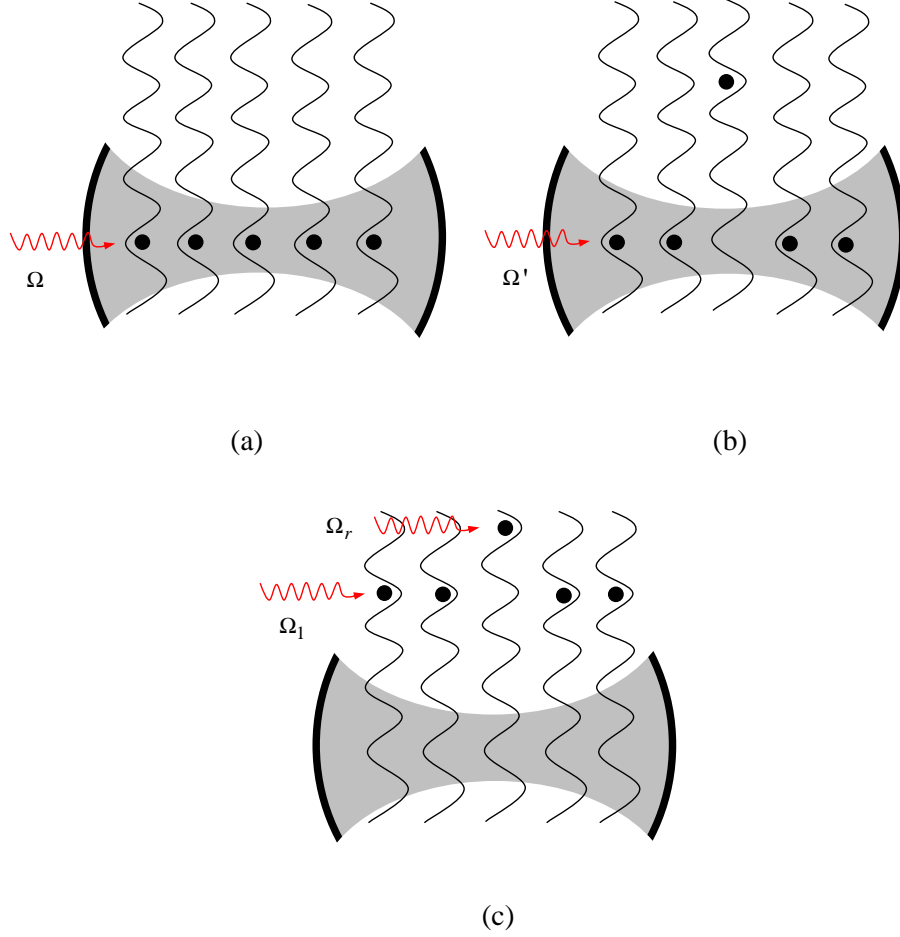


FIG. 9: Proposed set up for the NTCP gate performance with  $n + 1$  identical neutral atoms and a cavity. For simplicity, only five atoms are drawn here. Each atom can be loaded into the cavity or moved out of the cavity by one-dimensional (1D) translating optical lattices. The atom in the middle represents atom 1 (the control qubit) while the remaining atoms play the role of target qubits. In (a), a classical pulse with an initial phase  $\varphi = \pi$  and a Rabi frequency  $\Omega$  is applied to both of the control atom and the target atoms in the cavity; while in (b), a pulse with  $\varphi = 0$  and a Rabi frequency  $\Omega'$  is applied to the target atoms in the cavity. In (c), a pulse with  $\varphi = 0$  and a Rabi frequency  $\Omega_1$  is applied to the control atom while a pulse with  $\varphi = 0$  and a Rabi frequency  $\Omega_r$  is applied to the target atoms. Note that all of the pulses are resonant with the  $|0\rangle \leftrightarrow |1\rangle$  transition of each atom.

steps,  $n$  two-qubit controlled phase gates each described by the unitary transformation  $|\widetilde{00}\rangle \rightarrow |\widetilde{00}\rangle$ ,  $|\widetilde{01}\rangle \rightarrow |\widetilde{01}\rangle$ ,  $|\widetilde{10}\rangle \rightarrow |\widetilde{10}\rangle$ , and  $|\widetilde{11}\rangle \rightarrow -|\widetilde{11}\rangle$  are performed on the atom pairs  $(1, 2)$ ,  $(1, 3)$ , ..., and  $(1, n + 1)$ , respectively. Note that each pair contains the same control qubit (atom 1) but a different target qubit (atom 2, 3, ..., or  $n + 1$ ). Here and below, the states  $|\widetilde{0}\rangle$  and  $|\widetilde{1}\rangle$  are given by  $|\widetilde{0}\rangle = (|0\rangle + |1\rangle)/\sqrt{2}$  and  $|\widetilde{1}\rangle = (|0\rangle - |1\rangle)/\sqrt{2}$ , which have the same notation as those introduced in Section IV. A.

### B. Generation of multiqubit entangled states with atoms

To demonstrate the power of a NTCP gate, we now discuss how to create a multiqubit entangled state with atoms  $(1, 2, \dots, n + 1)$ , by using one cavity initially in an arbitrary state. The procedure introduced below for preparing multiple atoms in an entangled state is based on the above three steps for performing a NTCP gate with atoms. Note that different from previous works, our method below can be used to prepare multiple atoms in an entangled state *with an arbitrary entanglement degree* that varies with the initial state of the atom 1.

Consider  $(n + 1)$  identical two-level atoms  $(1, 2, \dots, n + 1)$  above. Each atom is trapped in periodic potential of an

one-dimensional optical lattice and can be loaded into or moved out of the cavity by translating the optical lattice. Suppose that atom 1 is in the state  $\alpha|\tilde{0}\rangle + \beta|\tilde{1}\rangle$  while atoms  $(2, 3, \dots, n+1)$  are all in the state  $|0\rangle$ . The initial state of the atomic system is thus given by

$$(\alpha|\tilde{0}\rangle + \beta|\tilde{1}\rangle) \otimes |0\rangle^{\otimes n}, \quad (62)$$

where the coefficients  $\alpha$  and  $\beta$  satisfy the normalization  $|\alpha|^2 + |\beta|^2 = 1$ . Note that  $|0\rangle = (|\tilde{0}\rangle + |\tilde{1}\rangle)/\sqrt{2}$ . Therefore, the state (62) can be written as

$$\frac{1}{2^{n/2}} \left[ \alpha|\tilde{0}\rangle \otimes (|\tilde{0}\rangle + |\tilde{1}\rangle)^{\otimes n} + \beta|\tilde{1}\rangle \otimes (|\tilde{0}\rangle + |\tilde{1}\rangle)^{\otimes n} \right]. \quad (63)$$

Now, we perform the three-step operations described above, which completes a phase flip (i.e.,  $|\tilde{1}\rangle \rightarrow -|\tilde{1}\rangle$ ) to the state  $|\tilde{1}\rangle$  of each of atoms  $(2, 3, \dots, n+1)$  when the control atom 1 is in the state  $|\tilde{1}\rangle$ . After that, it can be seen that the state (63) changes to

$$\alpha|\tilde{0}\rangle \otimes |0\rangle^{\otimes n} + \beta|\tilde{1}\rangle \otimes |1\rangle^{\otimes n}. \quad (64)$$

One can see that the state (64) is an entangled state of the  $(n+1)$  atoms  $(1, 2, \dots, n+1)$ . Note that the entanglement degree for this state varies when the magnitude  $|\alpha|$  or the magnitude  $|\beta|$  changes. For the case of  $|\alpha| = |\beta| = 1/\sqrt{2}$ , the state (64) becomes a well-known GHZ state which has the maximal entanglement and is of great importance in quantum information processing and quantum communication.

The state (64) is also an encoded state of the original state  $\alpha|\tilde{0}\rangle + \beta|\tilde{1}\rangle$  of atom 1, which shows that the quantum information originally carried by atom 1 has been encoded into or spread over the  $n+1$  atoms  $(1, 2, \dots, n+1)$ . As is well known, the state (64) is useful in quantum communication such as quantum secret sharing [47].

As shown above, the present scheme for implementing the NTCP gate or creating a multiqubit entangled state with atoms has the following features:

- (a) No adjustment of the level spacings for each atom is required during the entire operation;
- (b) Only one cavity is required;
- (c) The cavity mode can be initially in an arbitrary state;
- (d) The operation time does not depend on the number of atoms; and
- (e) The scheme presented here for preparing atoms in an entangled state is quite general, because as shown above it can be used to prepare  $(n+1)$  atoms in an entangled state with an *arbitrary* entanglement degree.

For our scheme to work: (i) the total cavity-atom interaction time  $\tau + \tau' = -2\pi/\delta + 2\pi/\delta'$  should be much smaller than the cavity decay time  $\kappa^{-1}$ , so that the cavity dissipation is negligible; and (ii) the  $\tau + \tau'$  needs to be much smaller than the energy relaxation time of the level  $|1\rangle$ , such that decoherence induced due to the spontaneous decay of the level  $|1\rangle$  is negligible. In principle, these conditions can be satisfied by choosing a cavity with a high quality factor  $Q$  and atoms with sufficiently long energy relaxation time.

## VII. CONCLUSIONS

We have presented two different methods for the proposed NTCP gate implementation. The two methods are quite general, which can be applied to physical systems such as trapped atoms, quantum dots, and superconducting qubits. There is no a priori preference between the two methods. The choice on them depends on the type of qubits used, and the technique available. For the two methods, we have provided detailed guidelines on how to protect multi-level qubits from leaking out of the computational subspace. As discussed in the appendixes, the leakage out of the computational subspace can in principle be suppressed as long as the cavity mode and the pulses are largely detuned from the transition between the irrelevant energy levels.

Using an concrete example, we have shown how to apply the first method to implement the NTCP gate with superconducting qubits coupled to a microwave resonator. In addition, we have discussed the experimental feasibility of performing a five-target-qubit controlled phase gate with superconducting qubits coupled to a one-dimensional transmission line resonator. Our analysis shows that the realization of this gate is possible within current technologies. We should mention that how well this gate would work in light of experimental errors should be further investigated. However, we note that it requires a rather lengthy and complex analysis, which is beyond the scope of this theoretical work.

We have shown how to extend the second method to implement the NTCP gate with trapped atomic qubits by the use of one cavity. Interestingly, it is noted that adjustment of the level spacings of atoms is not needed at all during the entire operation as shown above, and decoupling of atoms with the cavity can be easily achieved by just moving atoms out of the cavity. In addition, we have discussed how to prepare multiple atoms in an entangled state, by using one cavity initially in an arbitrary state. As shown above, the scheme presented above for preparing atoms in an entangled state is quite general, because it can be used to prepare  $(n + 1)$  atoms in an entangled state with an *arbitrary* entanglement degree.

In summary, we have presented a general proposal to implement a NTCP gate with qubits in a cavity or coupled to a resonator. As shown above, the present proposal has the following features: (i) The  $n$  two-qubit CP gates involved in the NTCP gate can be simultaneously performed; (ii) The operation time required for the gate implementation is independent of the number of the target qubits, thus it does not increase with the number of qubits; (iii) *The gate is insensitive to the initial state of the cavity mode, therefore no preparation for a specified initial state of the cavity mode is needed*; (iv) No measurement on the qubits or the cavity mode is needed and thus the operation is much simplified; (v) The detunings ( $\delta$  and  $\delta'$ ) are not required to be larger than the qubit-cavity coupling strengths ( $g$  and  $g'$ ); therefore a near-resonant interaction between the qubit and the cavity mode can be employed in order to reduce the error caused due to the transition from the qubit level  $|0\rangle$  or  $|1\rangle$  to other qubit levels; and (vi) *The gate realization requires only three steps of operations*. This proposal is quite general and can be applied to physical systems such as trapped atoms, quantum dots, and superconducting qubits. We believe that this work is of general interest and significance because it provides a protocol for performing a controlled-phase (or controlled-not) gate with multiple target qubits, which is important in quantum information processing.

### ACKNOWLEDGMENTS

F.N. and C.P.Y. acknowledges partial support from the National Security Agency (NSA), Laboratory for Physical Sciences (LPS), (U.S.) Army Research Office (USARO), National Science Foundation (NSF) under Grant No. 0726909, and JSPS-RFBR under Contract No. 06-02-91200. Y. X. L. acknowledges support from the National Natural Science Foundation of China under No. 10975080.

### APPENDIX A: HOW TO PROTECT QUBITS FROM LEAKING TO HIGHER ENERGY LEVELS FOR THE FIRST METHOD

Let us now discuss how to protect qubits from the leak out of the computational subspace in the presence of more qubit levels, for each step of the above operations. Generally speaking, we need consider two situations, which are here denoted as cases  $L$  and  $S$ . For case  $L$ , the level spacing between the level  $|1\rangle$  and the level  $|2\rangle$  (the first level above  $|1\rangle$ ) is *larger* than the level spacing between the levels  $|0\rangle$  and  $|1\rangle$ . Namely, for case  $L$ ,  $(E_2 - E_1) > (E_1 - E_0)$ , where  $E_0$ ,  $E_1$ , and  $E_2$  are the energy eigenvalues of the levels  $|0\rangle$ ,  $|1\rangle$ , and  $|2\rangle$ . For case  $S$ , the level spacing between the levels  $|1\rangle$  and  $|2\rangle$  is *smaller* than that between the levels  $|0\rangle$  and  $|1\rangle$ . Namely,  $(E_2 - E_1) < (E_1 - E_0)$ . For solid-state qubits, case  $L$  exists for superconducting charge qubits and flux qubits [16]; while case  $S$  can apply to superconducting phase qubits [19] and the so-called transmon design [48,49]. For atomic qubits, the level structures for both cases  $L$  and  $S$  are readily available. To simplify our presentation, we will focus on qubit 1 and discuss how to protect this qubit from the leak out of its computational subspace formed by the two logical states  $|0\rangle$  and  $|1\rangle$ . After that, we will give a brief discussion on how to protect the  $n$  target qubits  $(2, 3, \dots, n + 1)$  from the leakage.

#### A. Case L: $(E_2 - E_1) > (E_1 - E_0)$

For case  $L$ , let us consider Fig. 10(a), where the dashed line falls within the range between the levels  $|1\rangle$  and  $|2\rangle$  when the cavity mode is slightly detuned from the  $|0\rangle \leftrightarrow |1\rangle$  transition. Therefore, a large detuning of the cavity mode with the  $|1\rangle \leftrightarrow |2\rangle$  transition is needed to avoid the transition from the level  $|1\rangle$  to the level  $|2\rangle$ . Note also that as long as this large detuning is met, no transition from level  $|1\rangle$  to the higher energy level above the level  $|2\rangle$  happens. To explain this, let us consider an arbitrary level  $|a\rangle$  (with an energy eigenvalue  $E_a$ ) above the level  $|2\rangle$  [Fig. 10(a)]. Since the detuning  $\Delta_a = (E_a - E_1)/\hbar - \omega_c$  of the cavity mode with the  $|1\rangle \leftrightarrow |a\rangle$  transition is larger than the detuning  $\Delta_2 = (E_2 - E_1)/\hbar - \omega_c$  of the cavity mode with the  $|1\rangle \leftrightarrow |2\rangle$  transition, the large detuning  $\Delta_a$  of the cavity mode with the  $|1\rangle \leftrightarrow |a\rangle$  transition is automatically satisfied in the case when the large detuning  $\Delta_2$  of the cavity mode with the  $|1\rangle \leftrightarrow |2\rangle$  transition is met. As a result, the transition from the level  $|1\rangle$  to the level  $|a\rangle$  will not be induced by the cavity mode. In addition, the excitation of the level  $|a\rangle$ , induced due to its coupling to the level  $|2\rangle$  via the cavity mode, does not occur when the level  $|2\rangle$  is unpopulated. Hence, *as long as the large detuning  $\Delta_2$  of the cavity mode with the  $|1\rangle \leftrightarrow |2\rangle$  transition is satisfied, no level above  $|1\rangle$  will be populated and therefore the leak out of the computational subspace is suppressed*.

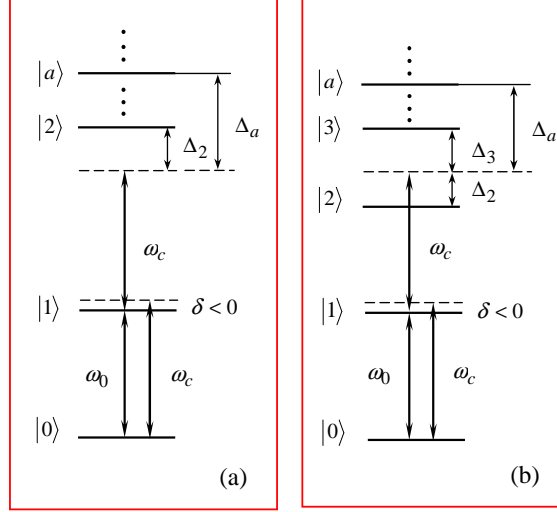


FIG. 10: Large detuning of the cavity mode with the transition between energy levels. Figure (a) corresponds to case  $L$  while figure (b) corresponds to case  $S$ . The dots above level  $|2\rangle$  in (a) and level  $|3\rangle$  in (b) represent other energy levels.  $\Delta_j = (E_j - E_1)/\hbar - \omega_c$  is the large detuning of the cavity mode with the  $|1\rangle \leftrightarrow |j\rangle$  transition ( $j = 2, 3$ , or  $a$ ). In (a),  $\Delta_a > \Delta_2$ ; while in (b),  $\Delta_a > \Delta_3$ .

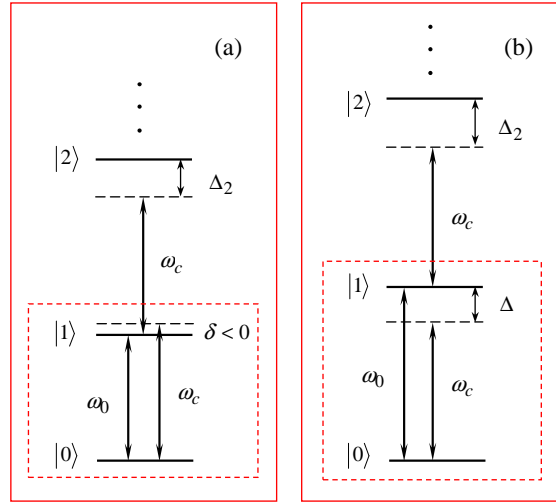


FIG. 11: (Color online) Illustration of the case when there is a large detuning  $\Delta_2 = (E_2 - E_1)/\hbar - \omega_c$  between the  $|1\rangle \leftrightarrow |2\rangle$  transition and the cavity mode for qubit 1 (with a multi-level structure belonging to case  $L$ ) during each step. Figure (a) is an extension of Fig. 3(a) to a multi-level case, which corresponds to step (i). Figure (b) is an extension of Fig. 3(b) or Fig. 3(c) to a multi-level situation, which corresponds to step (ii) or step (iii). In (a), the part enclosed in the (red) dashed-line box is the same as Fig. 3(a). In (b), the part enclosed in the (red) dashed-line box is the same as Fig. 3(b) or Fig. 3(c), and  $\Delta_2 > \Delta$ . Here,  $\Delta = (E_1 - E_0)/\hbar - \omega_c$  is the large detuning between the  $|0\rangle \leftrightarrow |1\rangle$  transition and the cavity mode.

By examining Figs. 3(a,b,c), we note that the large detuning  $\Delta_2$  of qubit 1 for each step of operations above can be achieved as follows. For step (i), it can be obtained by prior adjustment of the level spacings of qubit 1 before the gate [Fig. 11(a)]. For both step (ii) and step (iii), the large detuning  $\Delta_2$  of qubit 1 is automatically satisfied when tuning the qubit level spacings to have the cavity mode largely detuned from the  $|0\rangle \leftrightarrow |1\rangle$  transition [Fig. 11(b)]. This is because the level spacing between the levels  $|1\rangle$  and  $|2\rangle$  is larger than the  $|0\rangle \leftrightarrow |1\rangle$  level spacing for qubits belonging to case  $L$ , as mentioned above.

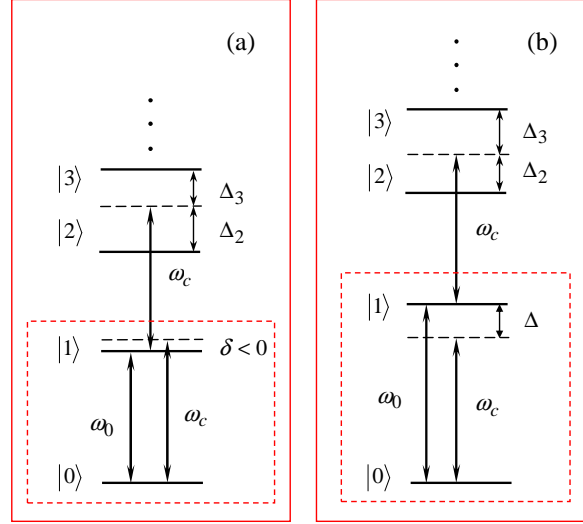


FIG. 12: (Color online) Illustration of the case when there are a large detuning  $\Delta_2 = (E_2 - E_1)/\hbar - \omega_c$  between the  $|1\rangle \leftrightarrow |2\rangle$  transition and the cavity mode, and a large detuning  $\Delta_3 = (E_3 - E_1)/\hbar - \omega_c$  between the  $|1\rangle \leftrightarrow |3\rangle$  transition and the cavity mode for qubit 1 (with a multi-level structure belonging to case  $S$ ) during each step. Figure (a) is an extension of Fig. 3(a) to a multi-level case, which corresponds to step (i). Figure (b) is an extension of Fig. 3(b) or Fig. 3(c), which corresponds to step (ii) or step (iii). In (a), the part enclosed in the (red) dashed-line box is the same as Fig. 3(a). In (b), the part enclosed in the (red) dashed-line box is the same as Fig. 3(b) or Fig. 3(c), and  $\Delta = (E_1 - E_0)/\hbar - \omega_c$  is the large detuning between the  $|0\rangle \leftrightarrow |1\rangle$  transition and the cavity mode.

### B. Case S: $(E_2 - E_1) < (E_1 - E_0)$

For case  $S$ , let us consider Fig. 10(b), where the dashed line falls within the range between the levels  $|2\rangle$  and  $|3\rangle$  when the cavity mode is slightly detuned from the  $|0\rangle \leftrightarrow |1\rangle$  transition. This can be achieved, e.g., for superconducting qubits by appropriately choosing the device parameters and/or adjusting the external parameters to control the level structures. From Fig. 10(b), it can be seen that a large detuning of the cavity mode with the  $|1\rangle \leftrightarrow |2\rangle$  transition and a large detuning of the cavity mode with the  $|1\rangle \leftrightarrow |3\rangle$  transition are needed to avoid the transition from the level  $|1\rangle$  to the level  $|2\rangle$  or the level  $|3\rangle$ . Note also that as long as these two large detunings are met, no transition from the level  $|1\rangle$  to the higher energy level above the level  $|3\rangle$  occurs. To understand this, let us consider an arbitrary level  $|a\rangle$  above  $|3\rangle$  [Fig. 10(b)]. Note that the detuning  $\Delta_a = (E_a - E_1)/\hbar - \omega_c$  of the cavity mode with the  $|1\rangle \leftrightarrow |a\rangle$  transition is larger than the detuning  $\Delta_3 = (E_3 - E_1)/\hbar - \omega_c$  of the cavity mode with the  $|1\rangle \leftrightarrow |3\rangle$  transition (here,  $E_3$  is the energy eigenvalue of the level  $|3\rangle$ ). Therefore, the large detuning  $\Delta_a$  of the cavity mode with the  $|1\rangle \leftrightarrow |a\rangle$  transition is automatically satisfied when the cavity mode is largely detuned from the  $|1\rangle \leftrightarrow |3\rangle$  transition. As a result, the transition from level  $|1\rangle$  to level  $|a\rangle$  will not be induced by the cavity mode. In addition, the excitation of the level  $|a\rangle$ , caused due to its coupling to the level  $|2\rangle$  or  $|3\rangle$  via the cavity mode, will not happen when the levels  $|2\rangle$  and  $|3\rangle$  are unpopulated. Hence, as long as the large detunings  $\Delta_2$  and  $\Delta_3$  are met, the levels above  $|1\rangle$  will not be excited by the cavity mode.

By examining Figs. 3(a,b,c), one can see that the large detunings  $\Delta_2$  and  $\Delta_3$  of qubit 1 for each step of the operations above can be obtained as follows. For step (i), the large detunings  $\Delta_2$  and  $\Delta_3$  can be achieved by prior adjustment of the level spacings of qubit 1 before the gate [Fig. 12(a)]. For step (ii) or step (iii), one can adjust the level spacings of qubit 1 to have a large  $\Delta_2$  and a large  $\Delta_3$  and to have the cavity mode largely detuned from the  $|0\rangle \leftrightarrow |1\rangle$  transition of qubit 1 [Fig. 12(b)], such that the states  $|0\rangle$  and  $|1\rangle$  of the qubit 1 are not affected by the cavity mode and no transition occurs from level  $|1\rangle$  to level  $|2\rangle$  or  $|3\rangle$ , or other levels above  $|1\rangle$ .

From the description above, it can be seen that to prevent qubits from leaking out of the computational subspace, only a large  $\Delta_2$  is required for qubits belonging to case  $L$  while both large  $\Delta_2$  and  $\Delta_3$  are needed for qubits belonging to case  $S$ . Therefore, the leak can be suppressed relatively easily for qubits belonging to case  $L$ .

For qubits belonging to case  $S$ , to avoid leaking out of the computational subspace, one would need a careful adjustment of the qubit level spacings (e.g., via appropriately choosing the external parameters and/or the device parameters) such that both large  $\Delta_2$  and  $\Delta_3$  can be met.

In the above, we have discussed how to protect qubit 1 from the leakage for each step. Now, let us briefly discuss how to protect the  $n$  target qubits ( $2, 3, \dots, n+1$ ) from the leakage for each step. For steps (i) and (ii), these  $n$  qubits can be protected from the leakage in the same way introduced above for protecting qubit 1 from the leakage for step

(i). This is because these  $n$  qubits have the same level structure as the control qubit 1 for step (i) [see Fig. 3(a) and Fig. 3(a')], and their level structure for step (ii) only has a small change when compared with their level structure for step (i) [Fig. 3(b') and Fig. 3(a')]. Therefore, from the discussion above for protecting qubit 1 from the leakage, it can be seen that in order to protect qubits  $(2, 3, \dots, n+1)$  from the leakage for steps (i) and (ii), a large detuning  $\Delta_2$  for case  $L$  [Fig. 11(a)] while a large  $\Delta_2$  and a large  $\Delta_3$  for case  $S$  [Fig. 12(a)] would be required for each of qubits  $(2, 3, \dots, n+1)$ . This requirement can be achieved by prior adjustment of the level spacings of the qubits  $(2, 3, \dots, n+1)$  before the gate operation.

In addition, note that for step (iii), qubits  $(2, 3, \dots, n+1)$  have the same level structure as the control qubit 1 for step (iii) [see Fig. 3(c) and Fig. 3(c')]. Thus, for this step (iii), qubits  $(2, 3, \dots, n+1)$  can be protected from the leakage by using the same manner introduced above for protecting qubit 1 from the leakage for step (iii). Namely, large detunings  $\Delta_2$  and  $\Delta$  for case  $L$  [Fig. 11(b)] while large detunings  $\Delta_2$ ,  $\Delta_3$  and  $\Delta$  for case  $S$  [Fig. 12(b)] will be needed for each of qubits  $(2, 3, \dots, n+1)$ . Note that this requirement can be obtained by adjustment of the level spacings of qubits  $(2, 3, \dots, n+1)$  during step (iii).

Finally, we should mention that adjustment of the level spacings of qubits  $(2, 3, \dots, n+1)$  *one by one* is not necessary since these  $n$  qubits have the same level structures for each step and thus their level spacings can be simultaneously adjusted (e.g., doable for solid state qubits), by changing their common external parameters.

## APPENDIX B: PROTECTING QUBITS FROM LEAKING TO HIGHER ENERGY LEVELS FOR THE SECOND METHOD

Let us now see how to protect multi-level qubits from leaking out of the computational subspace for each step of the operations above. Without loss of generality, we consider two cases, i.e., cases  $L$  and  $S$  above. For simplicity, we focus on qubit 1 and discuss how to protect this qubit from leaking out of its computational subspace. Note that the same argument can be applied to other qubits involved in the gate operation. As discussed before, to avoid leaking out of the computational subspace, we need a large  $\Delta_2$  for qubits belonging to case  $L$  while a large  $\Delta_2$  and a large  $\Delta_3$  for qubits belonging to case  $S$ .

For case  $L$ , the large  $\Delta_2$  of qubit 1 for each step above can be achieved as follows. For step (i), it can be achieved by prior adjustment of the level spacings of qubit 1 before the gate [Fig. 13(a)]. For step (ii), it is automatically met [Fig. 13(b)]. This is because the  $|0\rangle \leftrightarrow |1\rangle$  transition of qubit 1 was set to be largely detuned from the cavity mode during step (ii) [Fig. 4(b)], and the  $|1\rangle \leftrightarrow |2\rangle$  level spacing is larger than the  $|0\rangle \leftrightarrow |1\rangle$  level spacing for qubits belonging to case  $L$ . The same situation applies to step (iii) [Fig. 13(c)].

For case  $S$ , to obtain a large  $\Delta_2$  and  $\Delta_3$  of qubit 1 for each step above, one can follow this procedure. For step (i), both large  $\Delta_2$  and  $\Delta_3$  can be obtained [Fig. 14(a)], by prior adjustment of the level spacings of qubit 1 (doable with solid-state qubits) before the gate operation, or by appropriately choosing the qubit type (e.g., atomic qubits) to have the desired level structure. For step (ii), one will need a careful adjustment of the level spacings of qubit 1 to have the cavity mode largely detuned from the  $|0\rangle \leftrightarrow |1\rangle$  transition and to have the large  $\Delta_2$  and  $\Delta_3$  [Fig. 14(b)]. For step (iii), the leak of the computational subspace can be relatively easy to suppress because one can adjust the cavity-mode frequency to have a large  $\Delta_2$  [Fig. 14(c)]. Note that the  $|1\rangle \leftrightarrow |2\rangle$  level spacing is smaller than the  $|0\rangle \leftrightarrow |1\rangle$  level spacing for qubits belonging to case  $S$ . Therefore, the large detuning of the cavity mode with the  $|0\rangle \leftrightarrow |1\rangle$  transition of qubit 1, which is required by step (iii) [Fig. 4(c)], is automatically satisfied when tuning the cavity mode frequency to have a large  $\Delta_2$  [Fig. 14(c)].

From the description above, it can be seen that the leak out of the computational subspace can be readily suppressed for qubits belonging to case  $L$  since only a large  $\Delta_2$  is needed. With a careful adjustment of (a) the cavity mode frequency, (b) the level spacings for each qubit before the gate, and (c) the level spacing for qubit 1 during the gate, one can obtain both large  $\Delta_2$  and  $\Delta_3$  required by case  $S$  and thus the leakage for qubits belonging to case  $S$  can in principle be achieved.

In the above, we have discussed how to protect qubit 1 from the leakage for each step. Note that the  $n$  qubits  $(2, 3, \dots, n+1)$  have the same level structure as the control qubit 1 for step (i) [see Fig. 4(a) and Fig. 4(a')], and their level structure for step (ii) only has a small change when compared with their level structure for step (i) [Fig. 4(b') and Fig. 4(a')]. Therefore, qubits  $(2, 3, \dots, n+1)$  can be protected for steps (i) and (ii) in the same way presented above for protecting qubit 1 from the leakage for step (i). Namely, for protecting qubits  $(2, 3, \dots, n+1)$  from the leakage for step (i) or (ii), a large  $\Delta_2$  is required for each of these  $n$  qubits for case  $L$  [Fig. 13(a)] while a large  $\Delta_2$  and a large  $\Delta_3$  are needed for each of them for case  $S$  [Fig. 14(a)]. This requirement can be obtained by prior adjustment of the level spacings of qubits  $(2, 3, \dots, n+1)$  before the gate operation. In addition, note that for step (iii), the detuning  $\Delta$  is set to be the same for both of the control qubit 1 and the target qubits  $(2, 3, \dots, n+1)$  [Fig. 4(c) and Fig. 4(c')]. Hence, for step (iii), qubits  $(2, 3, \dots, n+1)$  belonging to case  $L$  are automatically protected from the leakage when the cavity mode frequency  $\omega_c$  is adjusted to have a large  $\Delta$  for qubit 1 and because  $\Delta_2$  is larger than  $\Delta$  for case  $L$  [Fig. 13(c)]. On the other hand, for step (iii), qubits  $(2, 3, \dots, n+1)$  belonging to case  $S$  are also automatically protected from the leakage, when tuning the cavity mode frequency  $\omega_c$  to have a large  $\Delta_2$  for qubit 1 and due to that  $\Delta$  is larger than



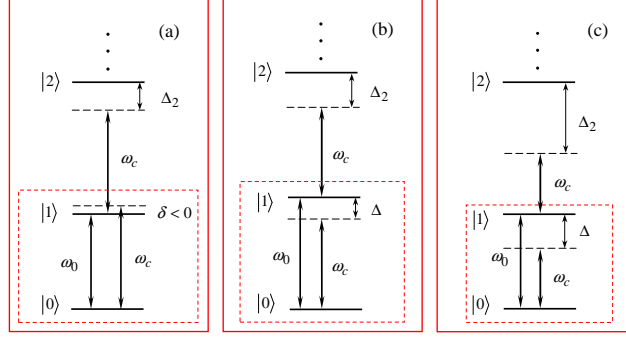


FIG. 13: (Color online) Illustration of the large detuning  $\Delta_2 = (E_2 - E_1)/\hbar - \omega_c$  for qubit 1 (with a multi-level structure belonging to case  $L$ ) during each step of the operations. Figures (a), (b), and (c) are extensions of Figs. 4(a,b,c) to a multi-level case, which correspond to steps (i), (ii), and (iii), respectively. In (a), (b), and (c), the parts enclosed in the (red) dashed-line boxes are in turn the same as Fig. 4(a), Fig. 4(b), and Fig. 4(c). In both (b) and (c),  $\Delta_2 > \Delta$ . Here,  $\Delta = (E_1 - E_0)/\hbar - \omega_c$  is the large detuning between the  $|0\rangle \leftrightarrow |1\rangle$  transition and the cavity mode.

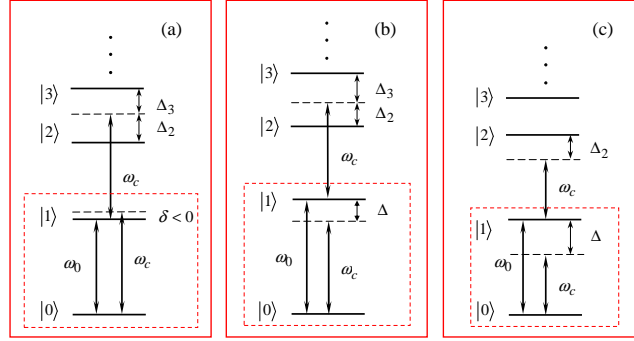


FIG. 14: (Color online) Illustration of the large detunings  $\Delta_2 = (E_2 - E_1)/\hbar - \omega_c$  and  $\Delta_3 = (E_3 - E_1)/\hbar - \omega_c$  for control qubit 1 (with a multi-level structure belonging to case  $S$ ) during each step. Figures (a), (b), and (c) are extensions of Figs. 4(a,b,c) to a multi-level case, which correspond to steps (i), (ii), and (iii), respectively. In (a), (b), and (c), the parts enclosed in the (red) dashed-line boxes are in turn the same as Fig. 4(a), Fig. 4(b), and Fig. 4(c). In both (b) and (c),  $\Delta = (E_1 - E_0)/\hbar - \omega_c$  is the large detuning between the  $|0\rangle \leftrightarrow |1\rangle$  transition and the cavity mode. In (c),  $\Delta_2 > \Delta$ .

$\Delta_2$  for case  $S$  [Fig. 14(c)]. From discussion given here, it can be seen that: *adjustment of the level spacings of the  $n$  target qubits ( $2, 3, \dots, n+1$ ) is not required during the entire three-step process for the second method.*

- 
- [1] Q. A. Turchette, C. J. Hood, W. Lange, H. Mabuchi, and H. J. Kimble, Phys. Rev. Lett. **75**, 4710 (1995).
  - [2] A. Rauschenbeutel, G. Nogues, S. Osnaghi, P. Bertet, M. Brune, J. M. Raimond, and S. Haroche, Phys. Rev. Lett. **83**, 5166 (1999).
  - [3] C. Monroe, D. M. Meekhof, B. E. King, W. M. Itano, and D. J. Wineland, Phys. Rev. Lett. **75**, 4714 (1995).
  - [4] J. A. Jones, M. Mosca, and R. H. Hansen, Nature (London) **393**, 344 (1998).
  - [5] X. Li, Y. Wu, D. Steel, D. Gammon, T. H. Stievater, D. D. Katzer, D. Park, C. Piermarocchi, and L. J. Sham, Science **301**, 809 (2003).
  - [6] T. Yamamoto, Yu. A. Pashkin, O. Astafiev, Y. Nakamura, and J. S. Tsai, Nature (London) **425**, 941 (2003).
  - [7] P. C. de Groot, C. J. P. M. Harmans, J. H. Plantenberg, and J. E. Mooij, Nature (London) **447**, 836 (2007).
  - [8] T. Monz, K. Kim, W. Hänsel, M. Riebe, A. S. Villar, P. Schindler, M. Chwalla, M. Hennrich, and R. Blatt, Phys. Rev. Lett. **102**, 040501 (2009).
  - [9] A. Barenco, C. H. Bennett, R. Cleve, D. P. DiVincenzo, N. Margolus, P. Shor, T. Sleator, J. A. Smolin, and H. Weinfurter, Phys. Rev. A **52**, 3457 (1995).
  - [10] M. Möttönen, J. J. Vartiainen, V. Bergholm, and M. M. Salomaa, Phys. Rev. Lett. **93**, 130502 (2004).
  - [11] C. P. Yang and S. Han, Phys. Rev. A **72**, 032311 (2005).
  - [12] L.-M. Duan, B. Wang, and H. J. Kimble, Phys. Rev. A **72**, 032333 (2005).
  - [13] X.-M. Lin, Z. W. Zhou, M. Y. Ye, Y. F. Xiao, and G. C. Guo, Phys. Rev. A **73**, 012323 (2006).

- [14] X. Wang, A. Sørensen, and K. Mølmer, Phys. Rev. Lett. **86**, 3907 (2001).
- [15] Y. Makhlin, G. Schön, and A. Shnirman, Rev. Mod. Phys. **73**, 357 (2001).
- [16] J.Q. You and F. Nori, Phys. Today **58** (11), 42 (2005).
- [17] J. Clarke and F. K. Wilhelm, Nature (London) **453**, 1031 (2008).
- [18] C. P. Yang, S. I. Chu, and S. Han, Phys. Rev. A **67**, 042311 (2003).
- [19] M. Neeley, M. Ansmann, R. C. Bialczak, M. Hofheinz, N. Katz1, E. Lucero, A. O'Connell, H. Wang, A. N. Cleland, and J. M. Martinis, Nature Physics **4**, 523 (2008).
- [20] For quantum dots, the level spacings can be changed via adjusting the external electronic field. For the details, see P. Pradhan, M. P. Anantram, and K. L. Wang, e-print arXiv:quant-ph/0002006 (unpublished).
- [21] M. Brune, E. Hagley, J. Dreyer, X. Maître, A. Maali, C. Wunderlich, J. M. Raimond, and S. Haroche, Phys. Rev. Lett. **77**, 4887 (1996).
- [22] M. Sandberg, C. M. Wilson, F. Persson, T. Bauch, G. Johansson, V. Shumeiko, T. Duty, and P. Delsing, Appl. Phys. Lett. **92**, 203501 (2008).
- [23] A. Palacios-Laloy, F. Nguyen, F. Mallet, P. Bertet, D. Vion, and D. Esteve, J. Low Temp. Phys. **151**, 1034 (2008).
- [24] J. R. Johansson, G. Johansson, C. M. Wilson, and F. Nori, Phys. Rev. Lett. **103** 147003 (2009).
- [25] J. Q. Liao, Z. R. Gong, L. Zhou, Yu-xi Liu, C. P. Sun, and F. Nori, e-print arXiv:quant-ph/0909.2748.
- [26] M. Šašura and V. Buzek, Phys. Rev. A **64**, 012305 (2001).
- [27] M. A. Nielsen and I. L. Chuang, Quantum Computation and Quantum Information (Cambridge University Press, Cambridge, England, 2001).
- [28] T. Beth and M. Rötteler, Quantum Information, Vol. **173**, Ch. 4, p. 96 (Springer, Berlin, 2001).
- [29] S. L. Braunstein, V. Buzek, and M. Hillery, Phys. Rev. A **63**, 052313 (2001).
- [30] S. B. Zheng, Phys. Rev. A **66**, 060303(R) (2002).
- [31] E. Solano, G. S. Agarwal, and H. Walther, Phys. Rev. Lett. **90**, 027903 (2003).
- [32] Z. J. Deng, M. Feng, and K. L. Gao, Phys. Rev. A **72**, 034306 (2005).
- [33] A. Sørensen and K. Mølmer, Phys. Rev. A **62**, 022311 (2000).
- [34] Y.D. Wang, P. Zhang, D. L. Zhou, and C. P. Sun, Phys. Rev. B **70**, 224515 (2004).
- [35] L. M. Duan, B. Wang, and H. J. Kimble, Phys. Rev. A **72**, 032333 (2005); A. Beige, D. Braun, B. Tregenna, and P. L. Knight, Phys. Rev. Lett. **85**, 1762 (2000).
- [36] J. A. Sauer, K. M. Fortier, M. S. Chang, C. D. Hamley, and M. S. Chapman, Phys. Rev. A **69**, 051804(R) (2004).
- [37] J. Q. You, J. S. Tsai, and F. Nori, Phys. Rev. Lett. **89**, 197902 (2002).
- [38] G. Falci, R. Fazio, G. M. Palma, J. Siewert, and V. Vedral, Nature (London) **407**, 355 (2000).
- [39] Y. Makhlin, G. Schn, and A. Shnirman, Nature (London) **398**, 305 (1999).
- [40] J. Q. You and F. Nori, Phys. Rev. B **68**, 064509 (2003).
- [41] J. Q. You, J. S. Tsai, and F. Nori, Phys. Rev. B **68**, 024510 (2003).
- [42] O. Astafiev, Y. A. Pashkin, Y. Nakamura, T. Yamamoto, and J. S. Tsai, Phys. Rev. Lett. **93**, 267007 (2004).
- [43] A. Wallraff, D. I. Schuster, A. Blais, L. Frunzio, J. Majer, M. H. Devoret, S. M. Girvin, and R. J. Schoelkopf, Phys. Rev. Lett. **95**, 060501 (2005).
- [44] A. Blais, R. S. Huang, A. Wallraff, S. M. Girvin, and R. J. Schoelkopf, Phys. Rev. A **69**, 062320 (2004).
- [45] D. I. Schuster, A. A. Houck, J. A. Schreier, A. Wallraff, J. M. Gambetta, A. Blais, L. Frunzio, J. Majer, B. Johnson, M. H. Devoret, S. M. Girvin, and R. J. Schoelkopf, Nature (London) **445**, 515 (2007).
- [46] P. K. Day, H. G. LeDuc, B. A. Mazin, A. Vayonakis, and J. Zmuidzinas, Nature (London) **425**, 817 (2003).
- [47] M. Hillery, V. Buzek, and A. Berthiaume, Phys. Rev. A **59**, 1829 (1999).
- [48] J. Koch, T. M. Yu, J. Gambetta, A. A. Houck, D. I. Schuster, J. Majer, A. Blais, M. H. Devoret, S. M. Girvin, and R. J. Schoelkopf, Phys. Rev. A **76**, 042319 (2007).
- [49] J. Q. You, X. Hu, S. Ashhab, and F. Nori, Phys. Rev. B **75**, 140515 (2007).